Science of the Total Environment 950 (2024) 175259

Contents lists available at ScienceDirect

Science of the Total Environment

journal homepage: www.elsevier.com/locate/scitotenv

Sharp decline in surface water resources for agriculture and fisheries in the Lower Mekong Basin over 2000-2020

Cassandra Normandin [a,*], Frédéric Frappart [a], Luc Bourrel [b], Fabien Blarel [c], Sylvain Biancamaria [c], Jean-Pierre Wigneron [a], Léonie Galenon [c], Emilie Bernard [c], Ludovic Coulon [c], Bertrand Lubac [d], Vincent Marieu [d], Vincent Vantrepotte [e], Binh Pham-Duc [f], Huy Toan Do [g,h], Catherine Prigent [i], Filipe Aires [i], Dai Yamazaki [j], Philippe Ciais [k]

[a] ISPA, UMR 1391 INRAE, Bordeaux Sciences Agro, F-33140 Villenave d'Ornon, France
[b] GET, Université de Toulouse, CNRS, IRD, UPS, CNES, OMP, Toulouse, France
[c] LEGOS, Université de Toulouse, CNES, CNRS, IRD, UPS, OMP, Toulouse, France
[d] EPOC, UMR 5805, Avenue des Facultés, Université de Bordeaux, 33405 Talence, France
[e] Univ. Lille, CNRS, Univ. Littoral Côte d'Opale, IRD, UMR 8187 - LOG - Laboratoire d'Océanologie et de Géosciences, 59000 Lille, France
[f] Department of Space and Applications, University of Science and Technology of Hanoi, Vietnam Academy of Science and Technology, Hanoi, Viet Nam
[g] World Wide Fund for Nature in Viet Nam, No 6 Lane 18 Nguyen Co Thach, Bac Tu Liem, Hanoi, Viet Nam
[h] Center For Environmental Fluid Dynamics, VNU University of Science, Hanoi, Viet Nam
[i] LERMA, Observatoire de Paris, CNRS, PSL, 61 avenue de l'Observatoire, 75 014 Paris, France
[j] Institute of Industrial Science, University of Tokyo, Komaba, Tokyo, Japan
[k] LSCE/IPSL, CEA-CNRS-UVSQ, Université Paris-Saclay, Gif-sur-Yvette, France

HIGHLIGHTS

- Spatio-temporal variability of surface water extent and volume over 2000–2020 in the Mekong Basin
- A strong decrease in the extent and volume of surface water and their links with climatic events
- A large decrease of the water residence time in the South of the Lower Mekong Basin
- Negative impacts of dam construction on surface water volume

GRAPHICAL ABSTRACT

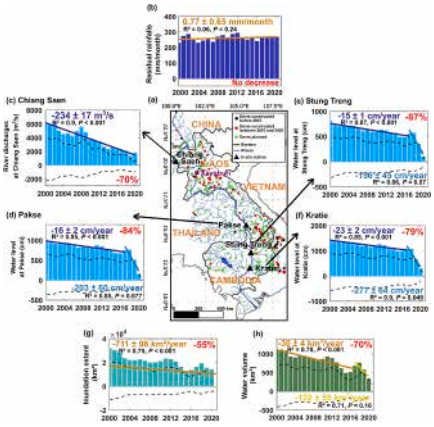

ARTICLE INFO

Editor: Martin Drews

ABSTRACT

Water resources play a crucial role in the global water cycle and are affected by human activities and climate change. However, the impacts of hydropower infrastructures on the surface water extent and volume cycle are

* Corresponding author.
E-mail address: cassandra.normandin@inrae.fr (C. Normandin).

https://doi.org/10.1016/j.scitotenv.2024.175259
Received 1 March 2024; Received in revised form 22 July 2024; Accepted 1 August 2024
Available online 8 August 2024
0048-9697/© 2024 The Authors. Published by Elsevier B.V. This is an open access article under the CC BY license (http://creativecommons.org/licenses/by/4.0/).

Keywords:
Remote sensing
Hydrology
Surface water volume
Dam operation
Flood

not well known. We used a multi-satellite approach to quantify the surface water storage variations over the 2000–2020 period and relate these variations to climate-induced and anthropogenic factors over the whole basin. Our results highlight that dam operations have strongly modified the water regime of the Mekong River, exhibiting a 55 % decrease in the seasonal cycle amplitude of inundation extent (from 3178 km^2 to 1414 km^2) and a 70 % decrease in surface water volume (from 1109 km^3 to 327 km^3) over 2000–2020. In the floodplains of the Lower Mekong Basin, where rice is cultivated, there has been a decline in water residence time by 30 to 50 days. The recent commissioning of big dams (2010 and 2014) has allowed us to choose 2015 as a turning point year. Results show a trend inversion in rice production, from a rise of 40 % between 2000 and 2014 to a decline of 10 % between 2015 and 2020, and a strong reduction in aquaculture growth, from +730 % between 2000 and 2014, to +53 % between 2015 and 2020. All these results show the negative impact of dams on the Mekong basin, causing a 70 % decline in surface water volumes, with major repercussions for agriculture and fisheries over the period 2000–2020. Therefore, new future projects such as the Funan Techo canal in Cambodia, scheduled to start construction at the end of 2024, will particularly affect 1300 km^2 of floodplains in the lower Mekong basin, with a reduction in the amount of water received, and other areas will be subjected to flooding. The human, material and economic damage could be catastrophic.

1. Introduction

Continental water storage plays a crucial role in the global water cycle, and its dynamics are essential for biodiversity and biogeochemical cycles. The extent and flow of inland waters also have a significant impact on human populations, economic activities, and societies (Shiklomanov and Rodda, 2003). However, in the last decades, water resources have increasingly been affected by the rapid growth of human activities (such as dam operations and reservoirs), and land areas have been impacted through extensive irrigation and urbanization (Arias et al., 2014; Kummu and Sarkkula, 2008; Lauri et al., 2012; Peñas and Barquín, 2019). Dams were identified as the most critical anthropogenic disturbances on continental surface waters (Li et al., 2017). >70 % of the world's largest rivers are affected by the operations of ~40,000 dams, and thousands more dams are planned in the coming years for hydropower production, which is likely to rise by 56 % globally in the next decades, but also for irrigation and flood control (Hecht et al., 2019; Nilsson et al., 2005; Poff and Schmidt, 2016; Zarfl et al., 2015). These human activities even impact the ecosystems in the world's most biodiverse regions such as the Amazon, Congo and Mekong River basins (Hecht et al., 2019; Winemiller et al., 2016). Environmental consequences on water quality, flood, agriculture, fishery, biodiversity, and sediment transport are critical (Bussi et al., 2021; Hecht et al., 2019; Yoshida et al., 2020).

The Mekong River, which is one of the largest rivers in the world is largely impacted by the dams located along the whole river. In fact, the Mekong's flow regime in the upper basin has seriously been affected by increasing of the dry season length and the dampening of the wet season flows, and a modification of the timing and magnitude of the Mekong flood pulse has already been detected (Hecht et al., 2019; Lauri et al., 2012; Piman et al., 2013; Pokhrel et al., 2018). The negative impact of dam structures on the hydrological cycle, as well as the societal and ecological effects, have been highlighted by studies mainly relying on hydrological modeling or statistical analysis based on observational data (Grumbine et al., 2012; Hecht et al., 2019; Johnston and Kummu, 2012; Li et al., 2017; Pokhrel et al., 2018). These studies have shown an abrupt alteration of the hydrological cycle in the Mekong during the last decade, but they were limited to the local/sub-basin scales as they were mostly based on *in situ* water levels and river discharge gauge records (Cochrane et al., 2014; Lu and Chua, 2021; Pham-Duc et al., 2019) or on results from hydrological models (Arias et al., 2014; Dang et al., 2022; Hoang et al., 2019; Lauri et al., 2012; Räsänen et al., 2017) with variable impacts on exposure and vulnerability to extreme droughts and floods (Kreibich et al., 2022, 2023). The use of a limited amount of *in situ* measurements of water levels or river discharges is not sufficient enough for large scale studies as *in situ* stations are do not allow to spatialize the hydrological variables monitored and offer either local-scale information or large-scale integrated hydrological variables. Besides, the maintenance costs of the *in-situ* networks and the time-delayed and limited data access in the case of transboundary river basins such as the Mekong River Basin (MRB) make the use of *in situ* hydrological measurements challenging (Grünwald et al., 2022; Wei et al., 2022).

Furthermore, these impacts are expected to be exacerbated with the occurrence of extreme floods and droughts in the future (Kreibich et al., 2022). Indeed, the study by Tang et al. (2024) summarized the impacts of climate change in the coming years on floods and droughts in the Mekong Basin. With regard to impacts on drought periods, Thilakarathne and Sridhar (2017) have shown an increase in the likelihood of severe drought scenarios throughout the basin, particularly in the Lower Mekong. This will result in an increase in the severity, duration and frequency of droughts throughout the Mekong basin in the coming years. In terms of flooding periods, the increase in precipitation over the Mekong basin between now and the end of the century will lead to more severe flooding, with an increase in high water levels of 13–30 %, an increase in peak flooded areas of 19–43 % and an increase in peak water volume of 24–55 % (Try et al., 2020). Other studies have investigated the projections over the coming decades of floods and droughts in this area (Dong et al., 2022; Kang et al., 2022; Li et al., 2021). The studies by Dong et al. (2022) and Li et al. (2021) showed an increase in humidity during wet periods and longer, more intense dry periods in the middle reaches of the Lower Mekong Basin. Decreasing precipitation and rising temperatures would be the primary drivers of this intensification of dry periods, but also of the increase in flash floods which will take place earlier in the year (June–July-August and September–October-November instead of December–January-February and March–April-May) over the whole Mekong Basin.

These sharp increases could be the cause of major human and economic losses (Tang et al., 2024).

Thus, better understanding the dynamics of the surface water volumes at the scale of the whole basin is crucial as changes in the upper part impact water resources downstream. The impacts on the hydrological cycle of the numerous infrastructures actually built on the river are still poorly known at the scale of the whole Mekong Basin. Allowing to overcome this issue, satellite remote sensing data offer unprecedented insights for evaluating the whole watershed across extended time periods. Satellite remote sensing makes it possible to quantify surface water volumes using various techniques (Papa and Frappart, 2021; Cretaux et al., 2023 for reviews). Synthetic Aperture Radar (SAR) interferometry (Alsdorf et al., 2007; Lu et al., 2019; Hong and Wdowinski, 2011; Kuenzer et al., 2013; Wdowinski et al., 2015; Pham-Duc et al., 2017) can be used to map height variations at high spatial resolution (<100 m) between two satellite passes, but is limited by low temporal repeatability and small surface areas. The other two techniques are based on combining flooded areas provided by satellite imagery with either terrain elevation models (DEMs) or radar altimetry. These approaches have mainly been used with flooded areas derived from passive microwaves (*e.g.*, using Global Inundation Estimate from Multiple Satellites (GIEMS), at 25 km spatial resolution (Prigent et al.,

2020; Bernard et al., 2024). Their main limitations are the low spatial resolution of the inundation maps and the limited temporal depth due to the use of altimetry data from a single mission (Frappart et al., 2015; Papa et al., 2015). These different methods are therefore unable to provide long time series of surface water volumes. To properly monitor the hydrological cycle of rivers, it is necessary to combine missions with suitable spatial and temporal resolution. To this end, more recent studies have made it possible to create longer time series (since 2000) using MODIS multi-spectral imagery (spatial resolution of 500 m and temporal resolution of 8 days) and altimetry missions in an Arctic environment, the Mackenzie Delta, between 2000 and 2015 (Normandin et al., 2018a), in a tropical basin, the Tonle Sap, between 1993 and 2016 (Frappart et al., 2018), the Mekong basin between 2003 and 2010 (Pham-Duc, 2018), and Inner Niger Delta between 2000 and 2020 (Normandin et al., 2024). These initial studies need to be extended to longer time series.

Despite the efforts made over the last two decades to quantify continental surface water using spatial remote sensing in the major river basins, long-term monitoring of surface water volumes remains limited. This gap raises major scientific questions, notably about the role of surface water in the global water cycle, but also about the impact of climate variability (interannual through extreme events, and long-term through climate change) and of human activity on a finer scale. Thus, the goal of this study is to quantify the spatio-temporal variations of surface water extents and volumes at the scale of the Mekong basin, including its upper and lower parts, during the 2000–2020 time period. We use a multi-satellite approach that combines multispectral imagery and radar altimetry to quantify surface water extents and water volumes over 2000–2020. Statistical tools are used to separate the signatures of long-term effects and extreme events, and to identify the most likely climate and anthropogenic factors which cause the changes in the water cycle. Impacts of the changes in surface water storage on food production are finally highlighted.

2. Study site

The Mekong River is one of the largest rivers in the world with a length of 4909 km, a drainage area of 795,000 km^2, and crosses six countries (China, Myanmar, Laos, Thailand, Cambodia and Vietnam) (Hecht et al., 2019; Hoang et al., 2019) (Fig. 1a). The Lower Mekong Basin is dominated by a tropical climate, characterized by the alternance of a wet season (lasting from May to October with an average of 1252 mm/year of cumulative rainfall) and a dry season (lasting from November to April with an average of 279 mm/month of cumulative rainfall). The region is a diverse ecosystem comprising various land types, including forest, cropland, grassland, sparse vegetation, permanently flooded and regularly flooded broadleaved forests (Fig. 1b). The Mekong River hosts the most productive inland fishery with >2 million tons of fish caught annually (Ziv et al., 2012). Moreover, it a crucial region for rice production, significantly contributing to global rice production (Ziv et al., 2012). Due to the rapid population growth in the basin, significant hydropower infrastructures have been developed primarily by China and Laos in the upper part of the basin, followed more recently by Vietnam and Thailand (Johnston and Kummu, 2012) (Fig. 1a). These infrastructures were designed for purposes such as hydropower production, irrigation, navigation, flood control, and water supply. However, they have significant impacts on both human and environment (Grumbine et al., 2012; Grumbine and Xu, 2011; Hecht et al., 2019), resulting in declines in fishery (Stone, 2016), alterations to sediment (Kondolf et al., 2014; Kummu and Varis, 2007) and nutrient transports (Chen et al., 2020), and changes to the geomorphology of floodplains in Cambodia and the coastal zone of Vietnam (Kummu and Varis, 2007).

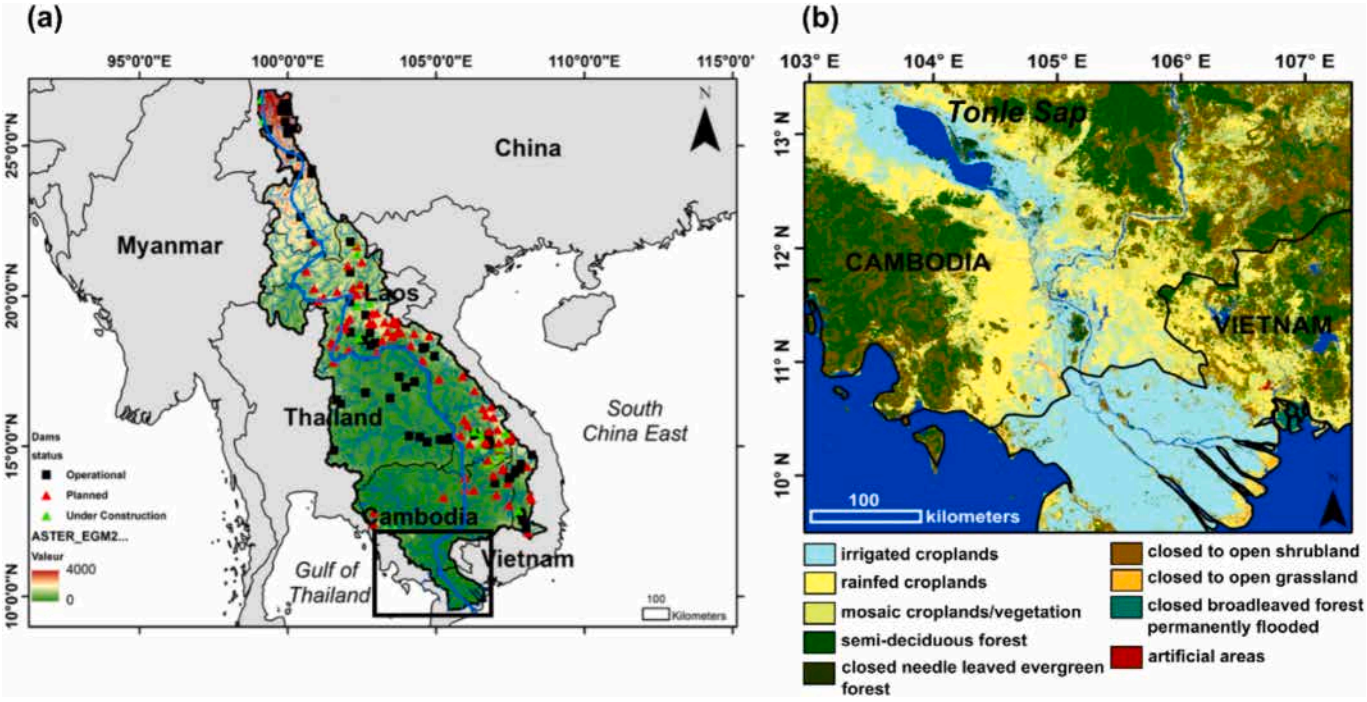

Fig. 1. Location of the Mekong basin with the associated vegetation map. a) Map of the Mekong River Basin, located in Southeast Asia. Dams are represented with symbols (black squares, red triangles, green triangles), corresponding to their status (operational, planned, under construction, respectively). Digital Elevation Model (DEM, in meters) is displayed as background. Black box in the downstream part of the basin represents the zoom shown on the right panel b), corresponding to the land cover (from http://due.esrin.esa.int/page_globcover.php) (Saah et al., 2020). Black dotted line represents the separation between the Upper Mekong Basin and Lower Mekong Basin (LMB).

3. Material and methods

3.1. Data

3.1.1. Multispectral imagery

The Moderate Resolution Imaging Sensor (MODIS), a spectroradiometer that operates on both Terra and Aqua satellites launched in 1999 and 2002, respectively, acquires daily images in 36 spectral bands at spatial resolution ranging from 250 to 1000 m. In this study, 8-day synthesis MOD09A1 level 3 product, version 6 product was employed. Specifically, the surface reflectance data from Terra have been freely downloaded from the United States Geological Survey (USGS) Earth Explorer website (https://search.earthdata.nasa.gov/search). In the 8-day product, each pixel contains the best observation during an 8-day period, based on a high observation coverage, low view angle, the absence of clouds and aerosol loading. Five tiles (h26v06, h27v06, h27v07, h28v07, h28v08) of 1200 × 1200 km are used to cover the Mekong Basin. For this study, a total of 941 composites have been used with a spatial resolution of 500 m and temporal resolution of 8 days over the period 2000–2020.

3.1.2. Radar altimetry

Water levels are derived from radar altimetry data from four different missions: ERS-2 (European Remote Sensing), ENVISAT (Environmental Satellite), SARAL (Satellite with ARgos and ALtika) and Sentinel-3 A and 3B. ERS-2, ENVISAT and SARAL satellites have a 35-day repeat cycle and were launched in 1995, 2002 and 2013 and ended in 2003, 2010 and 2016 respectively. Sentinel-3 A and 3B is a 27-day mission launched in 2016 by the European Space Agency (ESA). Altimetry data were made available by CTOH (Centre Topographie des Océans et de l'Hydrosphère, http://ctoh.legos.obs-mip.fr). More information on these missions can be found in (Frappart et al., 2021; Normandin et al., 2018a).

3.1.3. In situ river discharges and water levels

Daily *in situ* data of water levels and discharges of four stations (Chiang Saen (Thailand), Pakse (Laos), Stung Treng (Cambodia) and Kratie (Cambodia) are provided by the Mekong River Commission (https://portal.mrcmekong.org/home). Water levels were measured by manual (using a hydro pole) or automatic method (using radar sensor or pressure sensor). River discharges were also measured by manual (tachometer at representative hydrometer) or semi-automatic method (using ADCP equipment).

3.1.4. Climatic variables

3.1.4.1. Monthly rainfall. The Integrated Multi-satellitE Retrievals for Global Precipitation Monitoring (GPM IMERG) provides the multi-satellite precipitation product developed by the ASA GPM team (Huffman, 2019). The specific product used in this study is called « GPM IMERG Final Precipitation L3 1 month 0.1° x 0.1° V06 (GPM_3IMERGM) », which is freely available at https://giovanni.gsfc.nasa.gov/giovanni/.

3.1.4.2. Climatic indices. El Niño Southern Oscillation (ENSO) index is determined based on the anomalies of Sea Surface Temperature (SST) in different regions of the Pacific Ocean, spanning between longitude 120°W and 170°W and latitude 5°N and 5°S (Rayner, 2003). Data can be accessed at: https://www.esrl.noaa.gov/psd/gcos_wgsp/Timeseries/Nino34/.

The Pacific Decadal Oscillation (PDO) index is defined as the principal component of monthly Sea Surface Temperature variability in the North Pacific, poleward of 20°N (Mantua et al., 1997). Data is available at: https://www.esrl.noaa.gov/psd/gcos_wgsp/Timeseries/PDO/.

3.1.5. Other datasets

3.1.5.1. Evapotranspiration. The Global Land Evaporation Amsterdam Model (GLEAM) comprises a collection of algorithms designed to independently assess various elements of terrestrial evaporation, also known as "evapotranspiration", using satellite observations (Miralles et al., 2011). These elements include transpiration (Et), interception loss (Ei), bare-soil evaporation (Eb), snow sublimation (Es), and open-water evaporation (Ew). The version GLEAM V3.6 was used, which is a global dataset spanning 42-year period from 1980 to 2021, with a grid of 0.25° x 0.25° (Martens et al., 2016). The product is freely available at https://www.gleam.eu/.

3.1.5.2. Land cover maps. The annual land cover maps SERVIR-Mekong used in this study were generated by the Regional Land Cover Monitoring System (RLCMS), through a unique partnership between the U.S. Agency for International Development (USAID) and the U.S. National Aeronautics and Space Agency (NASA). All the data processing of Landsat and MODIS images to produce land cover maps are explained in details in (Poortinga et al., 2020; Saah et al., 2020). These maps consisted of 18 classes and have a spatial resolution of 600 m. They can be freely downloaded from: https://www.landcovermapping.org/en/landcover/.

The annual land use change maps used for the Mekong Delta used were processed by Vu et al. (2022b) and can be accessed online at: https://data.mendeley.com/datasets/kpftzmsyyz/2. The land use data maps are in GeoTiff format, cover the period between 2000 and 2020, and have a spatial resolution of 500 m. The land use classification consists of seven categories: inland aquaculture, shrimp-rice farming, others, single rice cropping, double rice cropping (mainly in the dry season and in the wet season) and triple rice cropping.

3.1.5.3. Rice production. The time series of rice production in the Mekong Delta from 2000 to 2020 was obtained from the General Statistics Office of Vietnam and is available for free download at: https://www.gso.gov.vn/en/homepage/.

3.2. Methods

3.2.1. Surface water extent

Spectral indices are frequently used with multispectral imagery to identify flood extent (Aires et al., 2020; Normandin et al., 2018b; Sakamoto et al., 2007). The method employed here is based on (Sakamoto et al., 2007) and has been improved and adapted by Normandin et al. (2018b, 2024, Fig. 2). This approach involves applying thresholds on the Enhanced Vegetation Index (EVI) and Land Surface Water Index (LSWI), defined as follow in (1) and (2) (Huete et al., 1997; Xiao et al., 2005):

$$\mathrm{EVI} = a \times \frac{\rho_{NIR} - \rho_{red}}{\rho_{NIR} + \mathrm{b} \times \rho_{red} - \mathrm{c} \times \rho_{blue} + \mathrm{d}} \quad (1)$$

$$\mathrm{LSWI} = \frac{\rho_{NIR} - \rho_{SWIR}}{\rho_{NIR} + \rho_{SWIR}} \quad (2)$$

With: _

- ρ_{red} is the surface reflectance value in the blue (621–670 nm, band 1)
- ρ_{NIR} is the surface reflectance value in the Near InfraRed (841–875 nm, band 2)
- ρ_{blue} is the surface reflectance value in the blue (459–479 nm, band 3)
- ρ_{SWIR} is the surface reflectance value in the Short-Wave InfraRed (1628–1652 nm, band 6)

Using these two spectral indexes, each pixel of one image is classified in one category: non-flooded or water related pixels (Fig. 2). Then, other

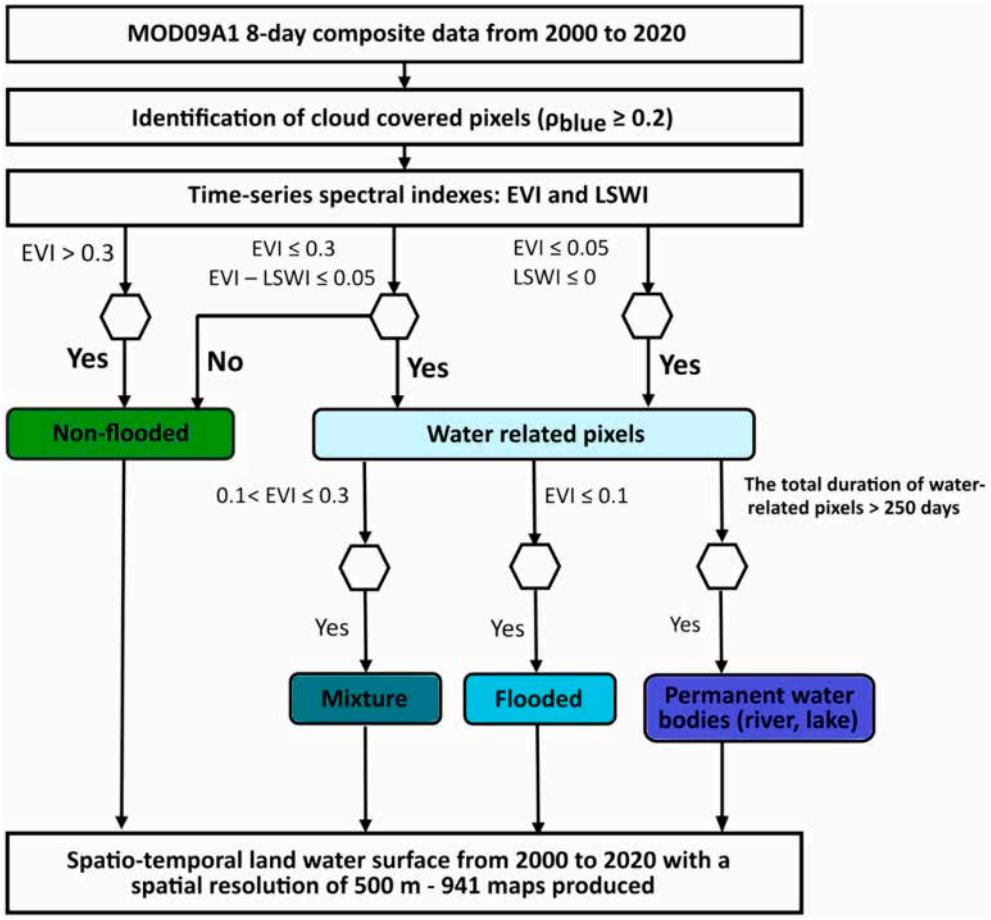

Fig. 2. Flow chart of the method (adapted from Sakamoto et al. (2007), modified after Normandin et al. (2018a, 2024)) used to classify each pixel of the multi-spectral images acquired over the Mekong Basin in four categories (non-flooded, mixed, flooded and permanent water bodies) for each year from 2000 to 2020 using MODIS 8-day composite at a spatial resolution of 500 m.

thresholds on EVI permit to classify water related pixels in mixture or flooded pixel. Finally, permanent water bodies (defined as river and lake) can be determined using a total duration of water related pixels superior to 250 days (Sakamoto et al., 2007). Using this method, spatio-temporal land water surface with a spatial resolution of 500 m have been studied using 941 maps over the whole period. Using the 941 inundations maps, monthly maps of inundation extent were produced and converted into a time series of inundation extent. The flow chart of the method is shown in Fig. 2.

3.2.2. *Water level time series*

Initially developed to measure ocean heights, radar altimeters have demonstrated their ability to study lake and river heights (Crétaux et al., 2017). Radar altimeters aboard satellites emit a radar signal towards the surface at nadir and measure the time taken for the echo to return to the altimeter. The technique enables the surface height to be determined based on the difference of the altitude of the satellite (called H) and the distance between the satellite and the surface or altimeter range (R_0). By subsequently applying various corrections to take account of atmospheric and geophysical effects, it is then possible to measure water heights on rivers and lakes, as defined in the following eq. (3, Frappart et al., 2021):

$$h = H - \left(R_0 + \Delta R_{iono} + \Delta R_{dry} + \Delta R_{solid\ Earth} + \Delta R_{pole}\right) - N \quad (3)$$

With:

- H: the surface height
- R_0: the distance between the satellite and surface (called altimeter range)
- ΔR_{iono}: is the atmospheric refraction range correction due to the free electron content associated with the dielectric properties of the ionosphere
- ΔR_{dry}: is the atmospheric refraction range correction due to the dry gas component of the troposphere
- $\Delta R_{solid\ Earth}$: corrections due to crustal vertical motions due to the solid Earth
- ΔR_{pole}: corrections due to crustal vertical motions due to pole tides
- N: geoid height

Since the launch of the first TOPEX altimetry mission in 1992, numerous altimetry missions have followed one another over the last three decades. This makes it possible to obtain temporal series of water heights over longer time series by combining missions, known as multi-missions (Berry et al., 2005; Schwatke et al., 2024; Tourian et al., 2016; Frappart et al., 2018; Normandin et al., 2018b; Shu et al., 2021). Numerous studies have been able to validate altimetric water levels from *in situ* data, such as in the Mackenzie Delta (Normandin et al., 2018a), in the Inner Niger Delta (Normandin et al., 2018b), the Ogooué Basin (Bogning et al., 2018), Swiss lakes (Frappart et al., 2021), the Lower Mekong Basin (Pham-Duc et al., 2019) and lakes in Sweden, Finland, Canada and the USA (Shu et al., 2021).

More explanations on the radar altimetry principle can be found in Chelton et al. (2001) and Escudier (2017). Specific processing to retrieve water levels over land is explained by Crétaux et al. (2017). Altimetry data were visualized and processed using the Multi-mission Altimetry

Processing Software (MAPS) (Frappart et al., 2015; Normandin et al., 2018a) for all missions except Sentinel-3 A and B and ALtimetry Time Series (ALTIS) software (Frappart et al., 2021) for Sentinel-3 A and B.

The processing involved four main steps (Normandin et al., 2018b):

(1) selecting cross-sections between river/lake and overlaying altimeter tracks using Google Earth,
(2) loading altimetry data over the Mekong Basin and the computation of the altimeter heights from the raw data contained in GDRs files,
(3) a refine selection of the valid altimetry data to remove outliers and measurements over non-water surface areas based on a visual inspection,
(4) creating of the time series of water levels.

The resulting time series, called Virtual Stations (*VS*), consisted of a dense network composed of 28, 32, 28 and 17 *VS* for ERS-2, ENVISAT, SARAL and Sentinel-3 A and B in the Mekong Basin.

3.2.3. Surface water volume storage

The estimation of surface water volume storage was accomplished by combining the surface water extent obtained from MODIS imagery with water levels calculated from radar altimetry data, as described in Normandin et al. (2018b). Water level maps were generated by interpolating water levels across water surface areas using an inverse-distance weighting spatial interpolation technique, similar to the method used in Frappart et al. (2006). However, due to the absence of altimetric missions between 2013 and 2016, there is a gap in the water level maps. Finally, the time series of surface water volume were computed for the Mekong Basin, following the approach of Frappart et al. (2006), using the following Eq. (4):

$$V = \sum_{j \in S} \left[h(\lambda_j, \varphi_j) - h_{\min}(\lambda_j, \varphi_j) \cdot \delta_j \cdot \Delta S \right] \quad (4)$$

where:

- V is the anomaly of surface water volume (km^3)
- S is the surface of the Mekong Basin (km^2)
- h (λ_j, φ_j) the water level for the pixel of coordinates (λ_j, φ_j) inside the Mekong Basin
- h_{min} (λ_j, φ_j) the minimal water level for the pixel of coordinates (λ_j, φ_j) inside the Mekong Basin
- δ_j equals 1 if the j^{th} pixel is associated with permanent water body or inundated pixel and 0 if not
- ΔS the pixel surface (0.25 km^2)

In order to fill the data gap between 2013 and 2016, a regression analysis was conducted between the time series of volumes and surface water extent from 2000 to 2013 and 2016–2020 (Fig. S1). The resulting regression equation was then utilized to estimate the surface water volumes for the period between 2013 and 2016 based on the available surface water extent data.

3.2.4. Statistical analyses

Statistical analysis has been performed on monthly time series of water surface and water volume using the Continuous Wavelet Transforms (CWT), Census-X11 decomposition and Principal Component Analysis (PCA).

First, the CWT is used to detect the periods and temporalities of the most energetic signals in a time series containing localized variations of power (*i.e.*, nonstationary) at various frequencies (Daubechies, 1990). The signal is decomposed at different frequencies using a so-called wavelet function and a scale-parameter (see Torrence and Compo, 1998) for an exhaustive presentation of the technique and its application in environmental sciences and for climatology purposes). The Cross Wavelet and Wavelet Coherence Toolbox (Grinsted et al., 2004) was used to perform the CWT. It is available at http://grinsted.github.io/wavelet-coherence/.

Then, a time series can be decomposed as X(t) = S(t) + T(t) + R(t), where S corresponds to the seasonal component, T the trend cycle, and R the residual component (Vantrepotte et al., 2011). This decomposition was performed here using Census-X11 algorithm, originally developed by (Pezzulli et al., 2005) for the analysis of sea surface temperature and then applied on ocean color data (Vantrepotte et al., 2011; Vantrepotte and Mélin, 2009). More details on this method can be found in (Vantrepotte and Mélin, 2009).

Finally, PCA is used to reduce the dimensionality of large dataset minimizing the loss of statistical information using the variance criteria (Jolliffe and Cadima, 2016). The maximization of the variance is based on the projection into a lower-dimensional space solving an eigen values/eigen vectors problem (Jolliffe and Cadima, 2016; Lever et al., 2017). This technique is commonly used for determining spatio-temporal modes of variability in environmental sciences (R, 1988).

4. Results

4.1. Time series of surface water extent and volume over 2000–2020 and their links with climatic events

Time series of inundation extent and surface water volumes anomalies over the Lower Mekong Basin (LMB) have been calculated and are shown in Fig. 3a and are compared with rainfall time series (Fig. 3b) and climate indices (Fig. 3c and d). Time series of surface water extent and volume are characterized by a strong seasonal cycle, with maximum values in August and minimum values in March/April (Fig. 3a). The slopes of the maximum values of the extent (indicated by the blue dotted line) and volumes (indicated by the orange dotted line) of surface water show a declining trend over time, with estimated decreases of 709 km^2/year (with a standard deviation of 192 km^2/year, coefficient of determination R^2 equals to 0.41 and *p*-value $P = 0.002$) and 3 km^3/year (with a standard error of 0.79 km^3/year, $R^2 = 0.43$ and $P = 0.001$), respectively (Fig. 2a.). In contrast, the minimum values show a lower slope, estimated at −56 km^2/year (with a standard error of 12 km^2/year, $R^2 = 0.54$ and $P = 0.001$) for the extent and − 0.0009 km^3/year (with a standard error of 0.08 km^3/year, $R^2 = 0.007$ and $P = 0.9$) for the volume (Fig. 3a).

Maximum values of the inundation extent and surface water volume in 2011 are associated with a negative ENSO and PDO. During this negative phase, an excess of rainfall (Fig. 3b) and subsequent flooding occurred in the summer due to the monsoon and anomalous hot temperatures over East Asia (Kim et al., 2014). On the contrary, minimum values in 2015 are due to a positive phase of ENSO (Fig. 3c) and PDO (Fig. 3d), leading to a rainfall deficit (Fig. 3b) and drought in the region during the following summer (Frappart et al., 2018). The impacts of climate events, and especially the combination of ENSO and PDO, have been well-documented in Southeast Asia, including the Tonle Sap, the largest lake of Southeast Asia, which is part of the LMB (Chen et al., 2021; Frappart et al., 2018; Nguyen et al., 2023). Lower interannual variability is observed when these two climate indices are out of phase.

4.2. A decrease in the surface water extent and volume and water time residence over 2000–2020

4.2.1. Decrease of the surface water extent and volume at the large basin scale

In order to identify the general trend in the time series of water surface area and volume over 2000–2020, various statistical analyses were applied (Fig. 4 for water volumes and Fig. S2 for water surface area).

First, the time series of surface water volumes was decomposed in three components using Census-X11 method: trend, seasonal and

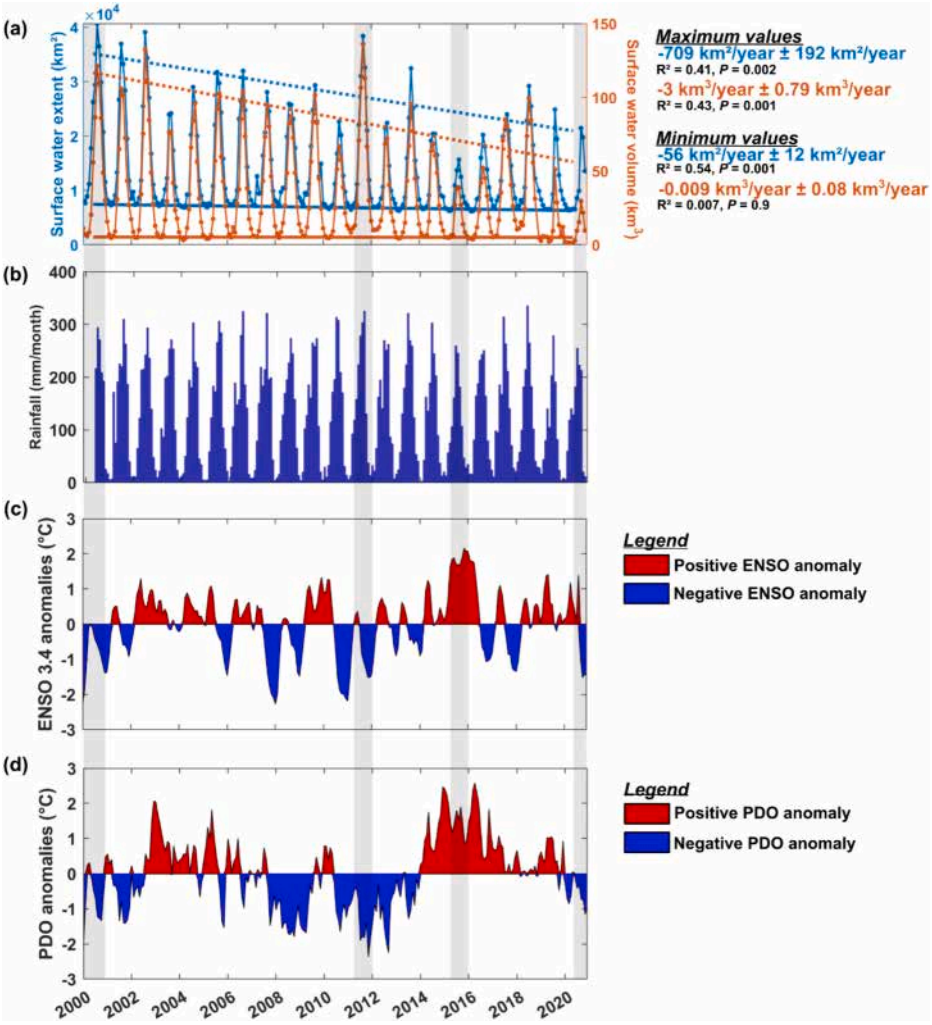

Fig. 3. Time series of the extent (km^2) and volumes (km^3) of surface water, rainfall (mm/month), and climatic indices ENSO and PDO anomalies (°C) over 2000–2020. a) Time series of surface water extent from multispectral imagery (km^2 - blue) and surface water volumes (km^3 – orange) over 2000–2020. For each time series, trend slopes of maximum values (dotted line) and minimum values (solid line) are displayed, -709 ± 192 km^2/year corresponds to a slope of -709 km^2/year and a standard error of 192 km^2/year with statistics (R^2 is the coefficient of determination and *P* is the *p*-value), b) time series of rainfall data from GPM over 2000–2020, c) time series of anomalies of ENSO 3.4 and d) time series of PDO (Pacific Decadal Oscillation) indices anomalies over 2000–2020. Grey rectangles represent minimum and maximum values of inundation extent and surface water volumes, with rainfall, ENSO and PDO associated.

residual components (Pezzulli et al., 2005; Vantrepotte et al., 2011). The analysis revealed a sharp decline in the seasonal cycle amplitude, with a 70 % reduction in magnitude, from 1109 km^3 to 327 km^3 (grey envelop in Fig. 4a). Time series of surface water extent show similar trends over 2000–2020 (Fig. S2a).

The PCA revealed that the first mode explained 57 % of the variance, while the second mode explained 12 % (Fig. 4b). Only the first and second temporal components displayed a clear seasonal signal and both exhibited a significant decreasing trend in seasonal amplitude over the entire time period. Spatial modes demonstrated that both permanent waterbodies (such as rivers and lakes, with positive values on both modes) and floodplains (positive values on the first mode and values close to 0 on the second mode) were impacted (Fig. 4c and 4d).

Finally, the CWT applied to the time series reveals a seasonal cycle with a large magnitude centred on a period of 1 year (characterized by a black envelop in Fig. S2b and S3). However, the width of this cycle strongly decreases over time, both in magnitude and duration, from 5 months at the beginning of the time series to 2–3 months in the last years (since 2012).

We highlighted the decrease in the seasonal cycle of the surface water extent (Fig. S2a) and volume anomalies (Fig. 4a) over 2000–2020 using three complementary statistical approaches (Census-X11, Continuous Wavelet Transform (CWT) and Principal Component Analysis (PCA), see Materials and Methods) to ensure the consistency of our analyses and provide complementary information. The Census-X11 method allows to study the time series as a whole, the Continuous Wavelet Transform (CWT) permits to study the duration and amplitude of phenomena, including for short time-periods with a duration of less than one year, and the Principal Component Analysis (PCA) to look at the spatial variations. All the three statistical analyses reveal evidence of extreme phenomena such as floods and droughts. The Census-X11 method identified the lowest surface water extent values in 2015 (drought) and highest values in 2011 (flood) (Fig. 4a). Large floods that occurred in 2001, 2002, 2011, and 2018 are clearly identifiable at the period of 6 months using the CWT method (Fig. S2b and S3). These extreme events of floods and droughts can also be detected in both the first two modes of PCA (Fig. 4b).

4.2.2. Decrease of the surface water extent and volume at the sub-basin scale

In the previous sub-section, an overall trend was observed in the temporal series of surface areas and volumes of water at the scale of the

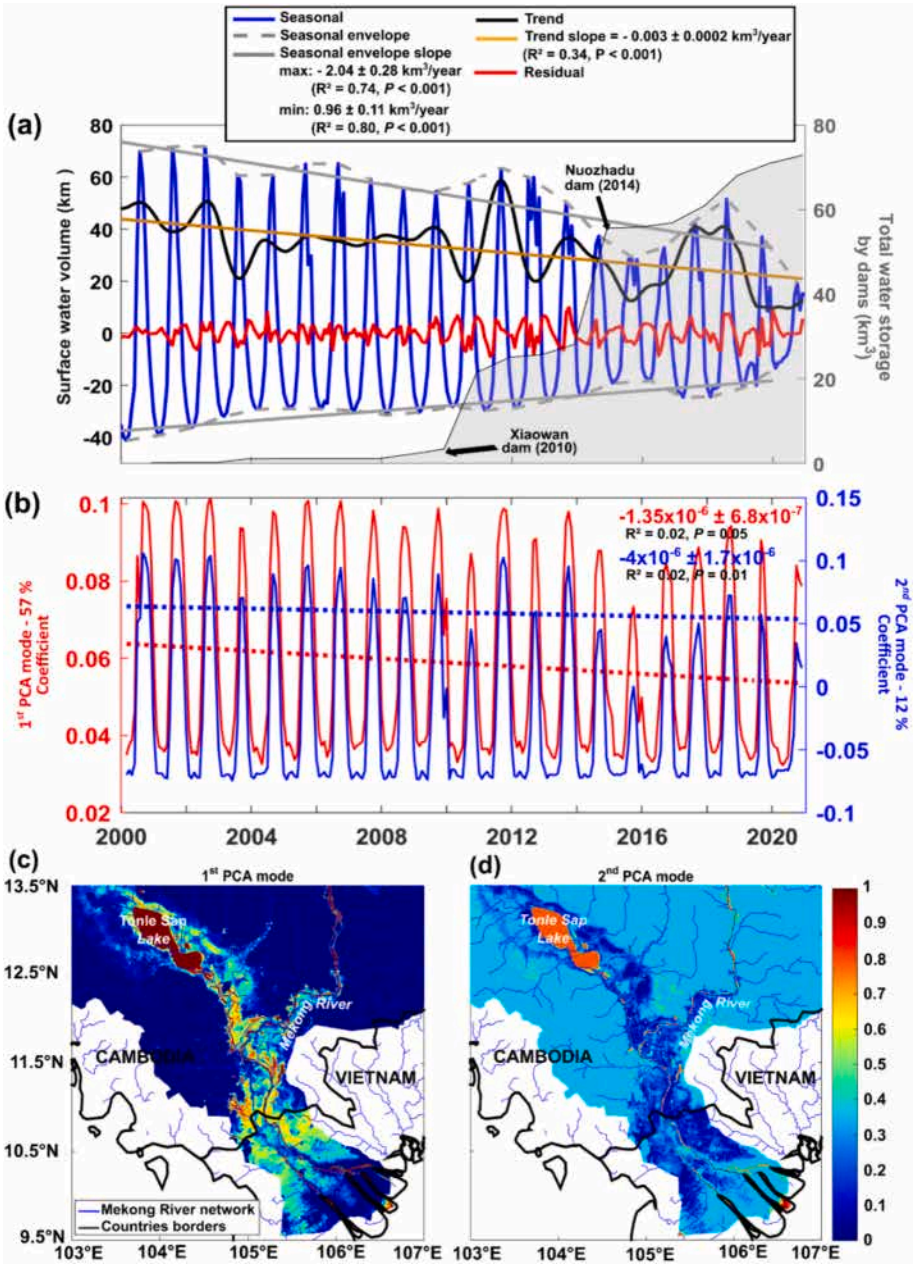

Fig. 4. Statistical analysis (Census X-11, PCA) applied to the surface water extent and volumes time series over 2000–2020 obtained from MODIS images at a spatial resolution of 500 m. a) Census-X11 decomposition of surface water volume. Grey area represents the total water storages by dams (km^3) with the commissioning of two large dams (Xiaowan and Nuozhadu built in 2010 and 2014, respectively), b) first and second modes of the PCA analysis of surface water extent with the trends in dotted lines. For each trend, slope and standard error with statistical parameters are shown: $-1.35 \times 10^{-6} \pm 6.8 \times 10^{-7}$ for the first mode, $-4 \times 10^{-6} \pm 1.7 \times 10^{-6}$ for the second mode), c) first principal spatial component of the PCA, d) second principal spatial component of the PCA.

Mekong basin (Fig. 5). Now, the temporal evolution of surface water extent and storage over 2000–2020 was examined in the seven sub-basins of the Mekong called R1, R2a, R2b, R2c, R3, R4 and R5 (as the rivers are not large enough in the upstream part of the Mekong basin, no time-series of water levels were generated in R1, R2a, b and c, and, hence, no storage variations were estimated in these sub-basins). As for the entire Mekong Basin, a Census-X11 decomposition on surface water extents and volumes was applied and presented in Fig. 5. Fig. 5a shows the location of the 7 sub-basins (R1, R2a, R2b, R2c, R3, R4 and R5) and dams along the Mekong River.

A decrease in the seasonal cycle of the surface water extent between 2000 and 2020 is observed in the different sub-basins. However, this decrease is not the same over the different sub-basins:

- a low decrease is observed in the upstream parts of the basin between 20° and 30° N: −2 % in both R1 and R2a,
- a medium one in the northwest part of Thailand (−22 % in R2b), and in the east of Cambodia and south east of Vietnam (−25 % in R4)
- a strong one in the west of Cambodia and southwest of Vietnam –(−45%in R5)
- very strong ones in the northeast and south of Thailand, and Laos (−58 % in R2c and − 79 % in R3)

A large decrease in the annual amplitude of surface water volume was also estimated: −87 % for R3, −32 % for R4 and − 59 % for R5. This strong decline is also confirmed by the CWT (the magnitude of the seasonal cycle, characterized by a black envelop centred on a period of 1 year in Fig. S4, strongly decreases in R3, 4 and 5, and almost completely

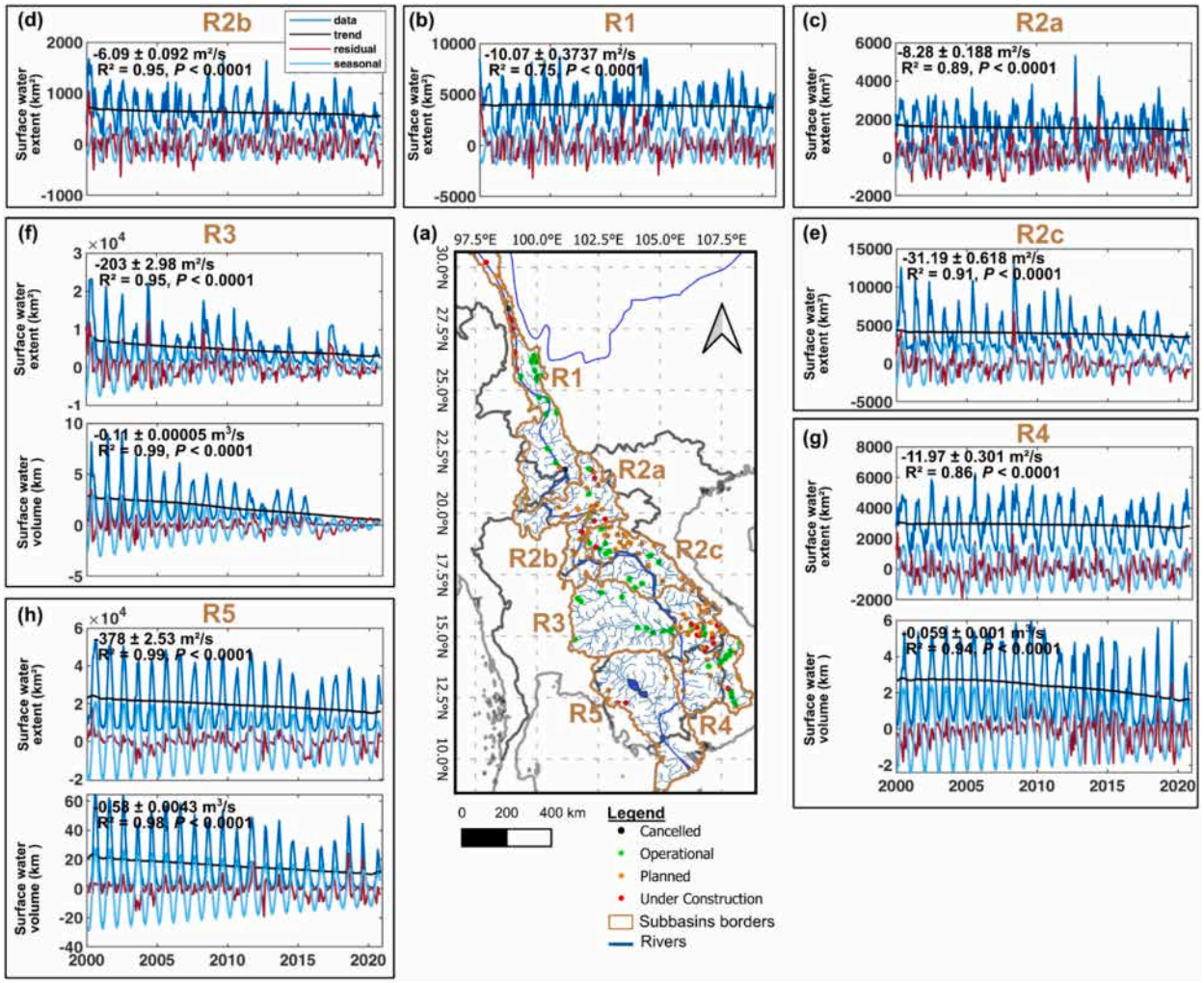

Fig. 5. Statistical analysis (Census X-11) applied to the surface water extent and volumes time series over 2000–2020 over sub-basins (numbered from R1 to R5): (a) Location of the sub-basins and dams (with black, green, red and orange dots), (b) R1, (c) R2a, (d) R2b, (e) R2c, (f) R3, (g) R4 and (h) R5. For each statistical decomposition, the data is in dark blue, the trend component in black, the seasonal component in light blue and the residual component in red. The slope of the trend, the coefficient of determination R^2 and the p-value *P* are displayed for each graph in black.

disappears after 2014 in R3).

4.2.3. A large decrease of the water residence time in the South of the Lower Mekong Basin (LMB)

After observing a sharp decrease in the amplitude and duration of the seasonal cycle of water surfaces and volumes at the scale of the Mekong basin and at the scale of the various sub-basins, we are going to study the variations spatially, and in particular in the downstream part of the Mekong basin, known as the Lower Mekong Basin. Flooding occurs in this part of the basin.

How did the decrease in the amplitude (Figs. 4a and b) and the duration (Fig. S2b) of the seasonal cycle revealed above affects the different regions of the LMB?

To illustrate the spatial distribution of this decrease, we estimated the difference in the number of days with water presence per year using maps of surface water extent between two periods: 2000–2009 and 2010–2020 (Fig. 6). The water residence time is defined as the duration of presence of water in each pixel of the study area every year. It is derived from the flood status provided by the processing of the MODIS eight-day synthesis over 2000–2020. We chose 2010 as the breaking point since new dams, including mega-dams with a water volume >10 km^3 such as Xiaowan (14.56 km^3) and Nuozhadu (23.70 km^3), were commissioned after this year. A clear gradient from upstream to downstream is evident in Fig. 6, with an increase of the annual flood duration of 30 days observed around the Tonle Sap lake (northwest) and a decrease southward in the Lower Mekong Basin. The reduction in annual flood duration is estimated to reach between 30 and 50 days in the Vietnam floodplains, which contain most of the irrigated croplands in the land cover maps (Saah et al., 2020) used in this study where rice is produced (Fig. 1b).

4.3. What are the causes of the decrease of surface water extent and volume and water residence time?

Statistical methods revealed a decrease in the seasonal amplitude of the surface water estimated at 55 % for inundation extent and 70 % for surface water volumes, suggesting that the hydrological cycle in the Mekong Basin has been impacted (Figs. 4, S2 and S3). Additionally, a decrease in water residence time in the southern LMB was observed, with an estimated average decrease of 30 to 50 days in the Vietnamese floodplains between 10°N and 11.5°N (Fig. 6).

What are the causes of these rapid changes that occurred over the last two decades?

Two main causes can be assumed: an anthropic and/or a climatic origin.

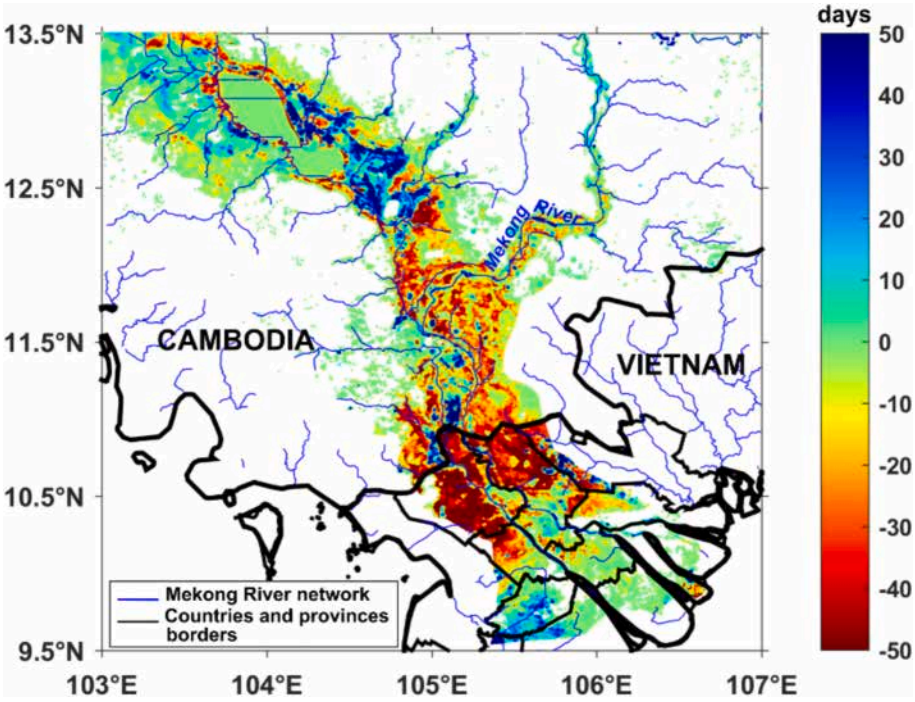

Fig. 6. Map of the difference between the number of days with occurrence of water for each pixel in a year between the two periods 2000–2009 and 2010–2020, in the Lower Mekong Basin. Blue values correspond to a positive difference between these two periods and red values to negative differences.

4.3.1. Climatic cause

To identify a possible climatic origin, a time series of monthly rainfall over the entire Mekong Basin was analyzed over the period 2000–2020 using the Census-X11 technique (Fig. 7b). The analysis, which involved decomposing the data into three components (trend, seasonal and residuals), revealed no reduction in the residual of annual rainfall cycle over the same period, calculated using monthly rainfall and evapotranspiration (Fig. 7b). Cumulative residual rainfall during both the wet (defined between May and October, Fig. S5a) and dry (defined between November and April, Fig. S5) seasons are slightly linearly related to the annual amplitude of surface water storage (Fig. 7g and 6h) over 2000–2020, as correlation coefficients of $R^2 = 0.57$ (*p*-value $P = 0.006$) and $R^2 = 0.46$ ($P = 0.04$), respectively, were obtained between their time-series. Correlation between the temporal variations of annual residual rainfall and annual amplitude of surface water storage is $R^2 = 0.43$ ($P = 0.05$). While the southwest monsoon was identified as the main contributor to the seasonal and annual variations in rainfall, interannual climatic events such as ENSO and PDO were also found to have an impact in the region (Frappart et al., 2018; Kummu and Sarkkula, 2008; Räsänen et al., 2017; Västilä et al., 2010). But the strong decline in surface water amplitude (60 km^3 over 2000–2020, which is equivalent to 70 % of the initial water volume (Fig. 4) is not observed in the residual of rainfall after evapotranspiration at annual time-scale nor during the wet period. Only small decrease in the residual of rainfall is observed during both the wet (−0.6 %/year) and the dry (−0.8 %/year) periods. Climate factors alone seem unable to account for the sharp decline in surface water extent and storage.

4.3.2. Anthropogenic cause

In the Mekong Basin, the construction of dams massively accelerated in the late 1990s (Cochrane et al., 2014; Lu and Chua, 2021). This strong increase in storage capacity (Fig. 7g and 7h) is partly caused by the commissioning of the large dams of Xiaowan (14.56 km^3) and Nuozhadu (23.70 km^3), built in 2010 and 2014, respectively. One of the main consequences highlighted by our results is a reduction in the duration of the flood in the central and lower parts of the basin (Fig. 6), confirmed by the decrease in the duration of the high water period recorded in the water levels and discharges from *in situ* stations of Chiang Saen (Thailand), Pakse (Laos), Stung Treng (Cambodia) and Kratie (Cambodia), respectively, all along the lower course of the Mekong River and downstream the two big dams mentioned previously (see Fig. 7a for their locations). Statistical analyzes were carried out on these *in situ* stations (Fig. 7c, d, e and f). We found the Chiang Saen station, shows a very strong decrease in the annual flow cycle, exhibiting a decrease in discharge from 6217 m^3/s to 1802 m^3/s between 2000 and 2020, *i.e.* a decrease of 70 % (Fig. 7c). The other three stations, located further downstream, also show a strong decrease in the seasonal cycle of water levels, of 84 % in Pakse, 87 % in Stung Treng and 79 % in Kratie (Fig. 6d, e and f respectively). The decrease of the annual cycle is stronger at Pakse, Stung Treng and Kratie, as they are located downstream of the construction of all dams (included Xiaowan and Nuozhadu) along the Mekong River (see Fig. 7a for their locations), in comparison to the *in situ* river discharges station of Chiang Saen, located downstream but close to the two mega-dams in the upstream part of the basin (Fig. 7c). The decrease over Pakse, Stung Treng and Kratie is linear over 2000–2017 and becomes more accentuated after 2018 until 2020, explained by the building of the big dam of Xayaburi (in 2019) downstream of the Chiang Saen station and upstream the three others (Fig. 7d, e and f). All these observations show the impact of the dam cascade along the Mekong River from China to Vietnam on the steep decrease of the annual cycle of the river flow as recorded by *in situ* data, but also on surface water extents and volumes over the whole Mekong Basin.

The number of dams in the Mekong basin has sharply risen since the late 1990s (Fig. 8). A strong acceleration in the number of dams in operation can be noted after 2011: 65 over the period 2011–2015 and then 72 over the period 2016–2020 against <30 for the three previous periods (before 1999, 2000–2005, 2006–2010, Fig. 8a). The increase is particularly noticeable in the R1, R2a, R2b and R2c sub-basins (Fig. 8a). In terms of capacity, across all sub-basins, it rises from 2565 MW before 1999, to 5155 MW over the period 2000–2005, then 14,579 MW over the period 2006–2010, then 24,153 MW over the period 2011–2016 and 35,802 MW over the period 2016–2020 (Fig. 8b). In comparison with the surface water extents and volumes over the period 2000–2020 shown in Fig. 5, a strong decrease in the seasonal cycle is observed,

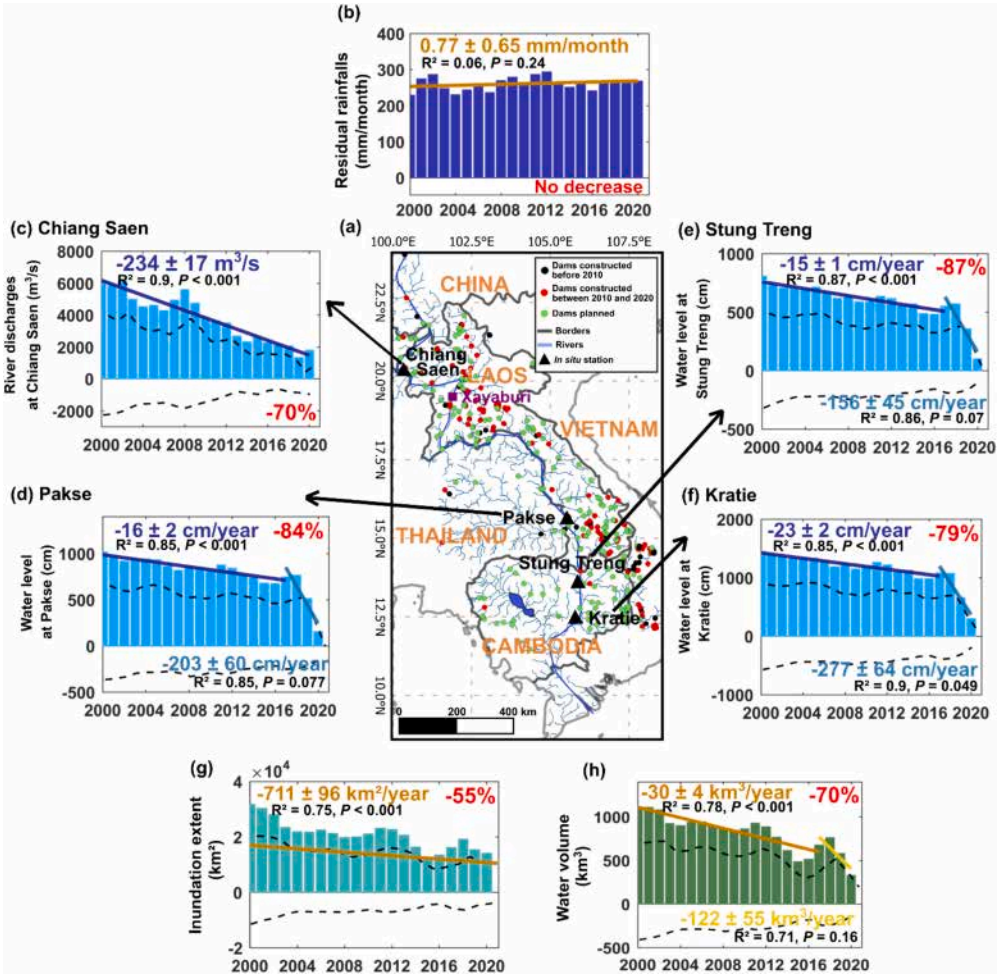

Fig. 7. Amplitude variations of the annual cycle (obtained by Census-X11 method) for surface water extent and volume, residual rainfall and comparison with *in situ* data. a) Map of the Mekong Basin showing dams locations. Barplot of the amplitude of the annual cycle using the Census-X11 decomposition for b) residual rainfall calculated using the difference between rainfall and evapotranspiration, c) river discharges (m^3/s) at Chiang Saen, water level (m) at d) Pakse, e) Stung Treng and f) Kratie, respectively, and for g) inundation extent (km^2) and h) water volume (km^3). For each barplot, dotted black points show minimum and maximum values of the cycle, blue (dark and light), orange and yellow straights are trends of the amplitude variations. Dams information came from https://monitor.mekongwater.org.

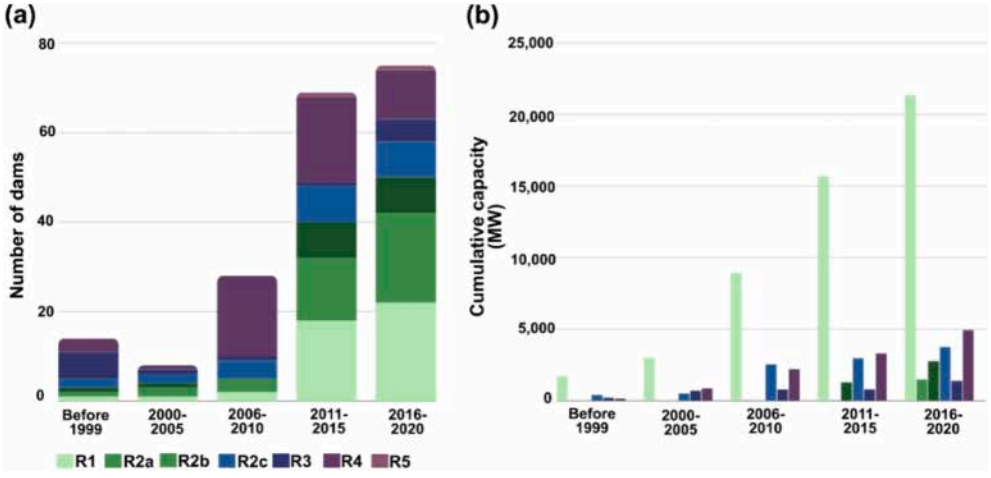

Fig. 8. Dams in the different sub-basins. (a) Number of dams for each sub-basin according different periods: before 1999, between 2000 and 2005, between 2006 and 2010, between 2011 and 2015 and between 2016 and 2020 and (b) the cumulative capacity (in MW) of dams for each sub-basin according the same periods defined previously. Dam data is from the Mekong River Commission website (https://portal.mrcmekong.org/hydropower/map) and the Mekong Dam Monitor website (https://monitor.mekongwater.org/).

particularly for the R3 sub-basin, estimated at −79 % for surface areas and − 87 % for volumes. On the other hand, for the different sub-basins, the decrease of the seasonal cycle is not the same:

- a weak decrease (−2 %) of surface water extent is observed in the upstream part of the Mekong River (around latitudes 20°N-30°N),a medium decrease (−22 % and − 25 %) is seen in the northwest of Thailand and Laos (sub-basin R2b) and in the east of Cambodia and the southeast of Vietnam (sub-basin R4)the strongest decrease (−45 % and − 58 %) is visible in the northeast of Thailand and Laos and the west of Cambodia and the southwest of Vietnam.

Surface water volumes for the R4 and R5 sub-basins are −32 and − 59 %. The very sharp decline observed for the R3 sub-basin can be directly related to the dams operating in the Chi and Mun basin which caused a decrease in discharge due to evaporation in the reservoirs and diversion of water for irrigation (Prakongsri and Santiboon, 2020).

To better account for the contribution of each factor (climatic or anthropogenic) on inundation extent and surface water volumes variations over the 2000–2020 period, hydrological and hydrodynamic modeling is required. A recent study in the Mekong River Basin, covering the period from 1979 to 2016, modeled several scenarios, including one that did not consider the effects of dams and another that did (Dang et al., 2022). This study found that dams had a growing influence on the Mekong flood pulse over time, with the greatest impact occurring after 2010, resulting in a 7 % reduction in discharge during peak flood events, as well as an effect on the Tonle Sap lake in the North, with a reduction in annual flood duration of 15 days in the lake's periphery and an increase in duration in the South. Our findings are consistent with those of the earlier study but are more pessimistic, exhibiting a 30-day reduction in annual flood duration along the Tonle Sap in the north and a 40-day increase in the south of the lake. This difference may be due to the different study periods (before 2016 for Dang et al., 2022), with our study covering more recent years when changes have been more abrupt. In addition to the impact on the Tonle Sap lake, our study also reveals that floodplains in the Lower Mekong Basin, specifically in Vietnam, have experienced a reduction in annual flooding duration by an average of 50 days since 2010.

The number of dams in the Mekong River Basin are projected to rise from 100 in 2020 to 140 in 2025, increasing water storage capacity from 65 to 90 km^3 (Hecht et al., 2019). Thus, the changes revealed, in this study, on the water regime of the LMB are likely to become more severe in the coming years.

5. Discussion

To evaluate the impacts of the decrease in surface water storage in amplitude and duration on agriculture, aquaculture and fisheries, maps of land use changes were used over the period 2000–2020 (Vu et al., 2022a). The main change observed was the transition from a double rice to a triple rice cropping in 2013 in the upstream and central regions of An Giang, Dong Thap, Long An, and Can Tho, which are the main rice-producing regions in the Mekong Delta (Fig. 9a and 9b).

Over the period 2000–2020, the amplitude of water surfaces decreased by 57 %, 51 %, 33 %, and 26 % for the regions of An Giang, Dong Thap, Long An, and Can Tho, respectively (Fig. 9d, f, h, and j). These regions are located in the most upstream part of the Vietnam delta.

With regard to rice production in these regions over the period 2000–2020, two trends can be observed:

- a sharp increase in production up to 2013 in the regions of An Giang (+84 %, Fig. 9c), Dong Thap (+77 %, Fig. 9e), Long An (+79 %, Fig. 9g) and a smaller increase in the Can Tho region (+15 %, Fig. 9i).

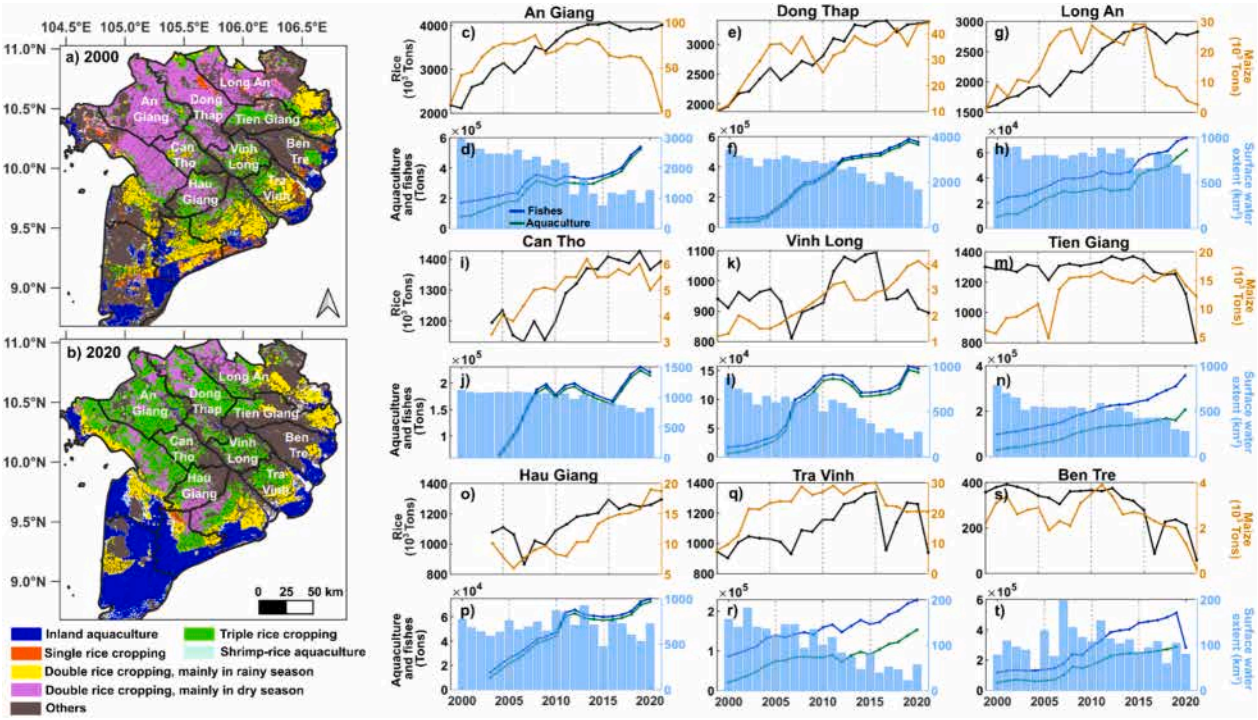

Fig. 9. Land use changes in the Vietnamese Mekong delta and time series of rice and maize production, aquaculture, fisheries and amplitude of surface water extent in nine provinces (An Giang, Dong Thap, Long An, Can Tho, Vinh Long, Tieng Giang, Hau Giang, Tra Vinh and Ben Tre) over 2000–2020. a) land use map in 2000 with seven classes (inland aquaculture, single rice cropping, double rice cropping in rainy and dry seasons, triple rice cropping, shrimp-rice cropping, others (from Vu et al., 2022a), b) land use map in 2020 (from Vu et al., 2022b). Rice, maize, aquaculture, fisheries and amplitude of surface water extent are displayed for each province: c), d) for An Giang, e), f) for Dong Thap, g), h) for Long An, i), j) for Can Tho, k), l) for Vinh Long, m), n) for Tien Giang, o), p) for Hau Giang, q), r) for Tra Vinh, s), t) for Ben Tre.

- a stagnation of rice production over the period 2014–2020, estimated at −0.2 % in An Giang (Fig. 9c), +1.4 % for Dong Thap (Fig. 9e), +0.5 % for Long An (Fig. 9g) and + 1.7 % for Can Tho (Fig. 9i).

For maize production, the same two periods (2000–2013 and 2014–2020) as for rice are identified:

- very strong increases in maize production between 2000 and 2013 for the regions of An Giang (+680 %, Fig. 9c), Dong Thap (+271 %, Fig. 9e), Long An (+1623 %, Fig. 9g) and Can Tho (+88 %, Fig. 9i) and a stagnation for the Dong Thap region (+13 %, Fig. 9e)
- a decrease in maize production for the An Giang (−97 %, Fig. 9c), Long An (−88 %, Fig. 9g) and Can Tho (−11 %, Fig. 9i) regions between 2014 and 2020

Thus, the transition from a double rice cropping to a triple rice cropping was not enough to counter the significant decrease of surface water extent, as a stagnation is observed across these four regions from 2013.

In contrast, in the central (Vinh Long, Tieng Giang, and Hau Giang) and downstream regions (Tra Vinh and Ben Tre), the triple rice harvest had already been used since 2000 (Fig. 9a and 9b). In these 5 regions:

- Rice production decreased over the period 2000–2020 (−5 %, −38 %, −0.5 %, −17 % for Vinh Long, Tien Giang, Tra Vinh and Ben Tre, respectively, Fig. 9k, m, q, s), except for Hau Giang where production increased by 20 % (Fig. 9o). Over the same period, water surfaces decreased by −68 %, −65 %, and − 63 % in the regions of Vinh Long, Tien Giang, and Tra Vinh (Fig. 9l, n, r), respectively, and by −6 % in Hau Giang (Fig. 9p)
- Maize production increased by 216 %, 96 %, 85 %, and 167 % in the regions of Vinh Long (Fig. 9k), Tien Giang (Fig. 9m), Hau Giang (Fig. 9o), and Tra Vinh (Fig. 9q) over 2000–2020. In Ben Tre, maize production decreased by 90 % (Fig. 9s), accompanied by a stagnation of water surfaces (+1.9 %, Fig. 9t).

Finally, aquaculture and fisheries appear to be also affected by the decrease in water surface extent. Significant growth is observed over the period 2000–2020 in the nine regions. However, this increase is more significant between 2000 and 2013, estimated on average at 730 % for aquaculture and 272 % for fisheries, than for the period 2014–2020, estimated on average at 53 % for aquaculture and 32 % for fisheries. In summary, maize production decreases in upstream regions and increases in central and downstream regions. Aquaculture and fisheries production increases more slowly after 2014. Rice production seems to be negatively impacted by the decrease in surface water storage, especially during the period of 2014–2020. The switch from a double to a triple rice harvest was not sufficient enough to counteract the decrease of surface water volume.

However, the stagnation observed in rice production after 2013 cannot be solely explained by the drop-in surface water volumes. As mentioned in (Van Kien et al., 2020), from the 1970s onwards, the Vietnamese government strongly encouraged farmers to develop their rice production, moving from double rice cropping to triple rice cropping, by offering financial aid to the various provinces. As a result, paddy rice production increased from 12.8 million tons in 1995 to 24.2 million tons in 2016 (Van Kien et al., 2020), but this high production involved poor quality rice. Unfortunately, the high production levels of previous decades have had a negative impact on soil quality through the intensive use of agricultural chemicals. In addition, the Mekong Delta is vulnerable to the effects of climate change, marked by saline intrusion and rising sea levels. All these factors have prompted the government to draw up a new plan to promote the flexible use of land for rice production by diversifying crop types, in order to obtain better quality rice. As a result, maize and aquaculture, in part, have considerably developed in recent years. It is therefore difficult to assess here the exact proportion due to the reduction in surface water volumes, and the proportion linked to the change in policy concerning rice production. As rice production sharply declined while maize production and fisheries and aquaculture either slowly increased or stagnated after 2013, it is more likely that the decrease in freshwater availability was a contributor to this inflexion in food production along with salinization of the Mekong Delta. However, all these changes in agriculture type has some positive impacts, especially on economy as the rice quality became better and the other type of agriculture earn more (Tran et al., 2018).

Finally, in addition to the construction of numerous dams in the coming years, new projects are appearing in the Mekong basin, such as the construction of the Funan Techo canal in Cambodia. Scheduled to start construction at the end of 2024 and to last 4 years, this canal will link the city of Phnom Penh to Kep (on the coast) *via* a 180 km long, 100 m wide channel. This canal will cross the lower Mekong, on the current floodplains between Vietnam and Cambodia (Eyler et al., 2024). The study by Eyler et al. (2024) presents the various impacts of this type of construction, particularly on surface water resources in the floodplains. They estimated that 1300 km^2 of floodplain areas bordering the canal to the south will be severely impacted by drying out. The presence of high-levee systems along the canal will prevent the passage of natural seasonal flooding on the other side. These areas will therefore receive a much lower amount of water. On the contrary, in the upstream part of the canal, new areas will be subject to flooding that were not previously. These include the town of Takeo City (104.78°E, 10.99°N, R5), the peri-urban areas of Phnom Penh (104.93°E, 11.55°N, R5) and the site of Techo international airport (104.94°E, 11.36°N, R5). The human, material and economic damage could be catastrophic.

6. Conclusion

This study showed a significant decrease in extent (55 %) and volume (70 %) of surface water in the Mekong basin over 2000–2020, as well as a drying out of 30 to 50 days in the floodplains of the lower Mekong. The results indicate that this decrease has most likely an anthropogenic origin, resulting from the construction of numerous large dams in the Upper Mekong Basin. Agriculture and aquaculture appear to be heavily impacted, with a stagnation in rice production (upstream regions) and a decrease in rice production (central and downstream regions). Maize production, on the other hand, is increasing (central and downstream regions) or stagnant (upstream regions). The future increase in dams number and water storage capacities is likely to worsen the situation for food production in the LMB and possibly be a threat to food security in the region.

Funding

Cassandra Normandin is funded by a CNES post-doctoral grant. This study was funded by the CNES SWOT grants SWHYM and WHYGHGS, and the Vietnam Academy of Science and Technology (VAST): grant number THTEXS.03-22/24 (BPD).

CRediT authorship contribution statement

Cassandra Normandin: Writing – review & editing, Writing – original draft, Visualization, Validation, Software, Resources, Methodology, Investigation, Formal analysis, Data curation, Conceptualization. **Frédéric Frappart:** Writing – review & editing, Writing – original draft, Supervision, Software, Funding acquisition, Conceptualization. **Luc Bourrel:** Writing – review & editing, Writing – original draft, Supervision, Methodology, Funding acquisition, Conceptualization. **Fabien Blarel:** Writing – review & editing, Validation, Software, Resources. **Sylvain Biancamaria:** Writing – review & editing. **Jean-Pierre Wigneron:** Writing – review & editing, Writing – original draft, Supervision, Methodology, Conceptualization. **Léonie Galenon:** Formal

analysis. **Emilie Bernard:** Formal analysis. **Ludovic Coulon:** Formal analysis. **Bertrand Lubac:** Writing – review & editing. **Vincent Vantrepotte:** Software, Resources. **Binh Pham-Duc:** Writing – review & editing, Validation, Methodology. **Huy Toan Do:** Validation. **Catherine Prigent:** Writing – review & editing. **Filipe Aires:** Writing – review & editing. **Dai Yamazaki:** Writing – review & editing. **Philippe Ciais:** Writing – review & editing, Methodology.

Declaration of competing interest

The authors declare that they have no known competing financial interests or personal relationships that could have appeared to influence the work reported in this paper.

Data availability

The datasets used and analyzed during the current study available from the corresponding author Cassandra Normandin on reasonable request.

Appendix A. Supplementary data

Supplementary data to this article can be found online at https://doi.org/10.1016/j.scitotenv.2024.175259.

References

Aires, F., Venot, J.-P., Massuel, S., Gratiot, N., Pham-Duc, B., Prigent, C., 2020. Surface water evolution (2001–2017) at the Cambodia/Vietnam border in the upper Mekong Delta using satellite MODIS observations. Remote Sens. 12, 800. https://doi.org/10.3390/rs12050800.

Alsdorf, D.E., Rodríguez, E., Lettenmaier, D.P., 2007. Measuring surface water from space. Rev. Geophys. 45 (2).

Arias, M.E., Piman, T., Lauri, H., Cochrane, T.A., Kummu, M., 2014. Dams on Mekong tributaries as significant contributors of hydrological alterations to the Tonle Sap floodplain in Cambodia. Hydrol. Earth Syst. Sci. 18, 5303–5315. https://doi.org/10.5194/hess-18-5303-2014.

Bernard, J., Prigent, C., Jimenez, C., Frappart, F., Normandin, C., Zeiger, P., Peng, S., 2024. Assessing the time variability of GIEMS-2 satellite-derived surface water extent over 30 years. Front. Remote Sens. 5, 1399234.

Berry, P.A.M., Garlick, J.D., Freeman, J.A., Mathers, E.L., 2005. Global inland watermonitoring from multi-mission altimetry. Geophys. Res. Lett. 32 (16).

Bogning, S., Frappart, F., Blarel, F., Niño, F., Mahé, G., Bricquet, J.P., Braun, J.J., 2018. Monitoring water levels and discharges using radar altimetry in an ungauged river basin: The case of the Ogooué. Remote Sens. 10 (2), 350.

Bussi, G., Darby, S.E., Whitehead, P.G., Jin, L., Dadson, S.J., Voepel, H.E., Vasilopoulos, G., Hackney, C.R., Hutton, C., Berchoux, T., Parsons, D.R., Nicholas, A., 2021. Impact of dams and climate change on suspended sediment flux to the Mekong delta. Sci. Total Environ. 755, 142468. https://doi.org/10.1016/j.scitotenv.2020.142468.

Chelton, D.B., Ries, J.C., Haines, B.J., Fu, L.-L., Callahan, P.S., 2001. Chapter 1 Satellite Altimetry. International Geophysics. Elsevier, in, pp. 1–ii. https://doi.org/10.1016/S0074-6142(01)80146-7.

Chen, A., Liu, J., Kummu, M., Varis, O., Tang, Q., Mao, G., Wang, J., Chen, D., 2021. Multidecadal variability of the Tonle Sap Lake flood pulse regime. Hydrol. Process. 35 https://doi.org/10.1002/hyp.14327.

Chen, Q., Shi, W., Huisman, J., Maberly, S.C., Zhang, J., Yu, J., Chen, Y., Tonina, D., Yi, Q., 2020. Hydropower reservoirs on the upper Mekong River modify nutrient bioavailability downstream. Natl. Sci. Rev. 7, 1449–1457. https://doi.org/10.1093/nsr/nwaa026.

Cochrane, T.A., Arias, M.E., Piman, T., 2014. Historical impact of water infrastructure on water levels of the Mekong River and the Tonle Sap system. Hydrol. Earth Syst. Sci. 18, 4529–4541. https://doi.org/10.5194/hess-18-4529-2014.

Cretaux, J.F., Calmant, S., Papa, F., Frappart, F., Paris, A., Berge-Nguyen, M., 2023. Inland surface waters quantity monitored from remote sensing. Surv. Geophys. 44 (5), 1519–1552.

Crétaux, J.-F., Nielsen, K., Frappart, F., Papa, F., Calmant, S., Benveniste, J., 2017. Hydrological applications of satellite AltimetryRivers, lakes, man-made reservoirs, inundated areas. Satellite altimetry over oceans and land surfaces 459–504.

Dang, H., Pokhrel, Y., Shin, S., Stelly, J., Ahlquist, D., Du Bui, D., 2022. Hydrologic balance and inundation dynamics of Southeast Asia's largest inland lake altered by hydropower dams in the Mekong River basin. Sci. Total Environ. 831, 154833 https://doi.org/10.1016/j.scitotenv.2022.154833.

Daubechies, I., 1990. The wavelet transform, time-frequency localization and signal analysis. IEEE Trans. Inf. Theory 36, 961–1005. https://doi.org/10.1109/18.57199.

Dong, Z., Liu, H., Hu, H., Khan, M.Y.A., Wen, J., Chen, L., Tian, F., 2022. Future projection of seasonal drought characteristics using CMIP6 in the Lancang-Mekong River basin. J. Hydrol. 610, 127815.

Escudier, P., 2017. Satellite Radar Altimetry | 1 | Principle, Accuracy, and Precision | P [WWW Document]. URL. https://www.taylorfrancis.com/chapters/edit/10.1201/9781315151779-1/satellite-radar-altimetry-philippe-escudier-alexandre-couhert-flavien-mercier-alain-mallet-pierre-thibaut-ngan-tran-la%C3%AFba-amarouche-bruno-picard-loren-carrere-g%C3%A9rald-dibarboure-micha%C3%ABl-ablain-jacques-richard-nathalie-steunou-pierre-dubois-marie-h%C3%A9l%C3%A8ne-rio-jo%C3%ABl-dorandeu (accessed 5.11.23).

Eyler, B., Kwan, R., Weatherby, C., 2024. May 9. Impacts of Cambodia's Funan Techo Canal and implications for Mekong cooperation, Stimson Center.

Frappart, F., Minh, K.D., L'Hermitte, J., Cazenave, A., Ramillien, G., Le Toan, T., Mognard-Campbell, N., 2006. Water volume change in the lower Mekong from satellite altimetry and imagery data. Geophys. J. Int. 167, 570–584. https://doi.org/10.1111/j.1365-246X.2006.03184.x.

Frappart, F., Fatras, C., Mougin, E., Marieu, V., Diepkilé, A.T., Blarel, F., Borderies, P., 2015. Radar altimetry backscattering signatures at Ka, Ku, C, and S bands over West Africa. Physics and Chemistry of the Earth, Parts A/B/C, Emerging science and applications with microwave remote sensing data 83–84, 96–110. https://doi.org/10.1016/j.pce.2015.05.001.

Frappart, F., Biancamaria, S., Normandin, C., Blarel, F., Bourrel, L., Aumont, M., Azemar, P., Vu, P.-L., Le Toan, T., Lubac, B., Darrozes, J., 2018. Influence of recent climatic events on the surface water storage of the Tonle Sap Lake. Sci. Total Environ. 636, 1520–1533. https://doi.org/10.1016/j.scitotenv.2018.04.326.

Frappart, F., Zeiger, P., Betbeder, J., Gond, V., Bellot, R., Baghdadi, N., Blarel, F., Darrozes, J., Bourrel, L., Seyler, F., 2021. Automatic detection of inland water bodies along altimetry tracks for estimating surface water storage variations in the Congo Basin. Remote Sens. 13, 3804.

Grinsted, A., Moore, J.C., Jevrejeva, S., 2004. Application of the cross wavelet transform and wavelet coherence to geophysical time series. Nonlinear Process. Geophys. 11, 561–566. https://doi.org/10.5194/npg-11-561-2004.

Grumbine, R.E., Xu, J., 2011. Mekong Hydropower Development. Science 332, 178–179. https://doi.org/10.1126/science.1200990.

Grumbine, R.E., Dore, J., Xu, J., 2012. Mekong hydropower: drivers of change and governance challenges. Front. Ecol. Environ. 10, 91–98. https://doi.org/10.1890/110146.

Grünwald, R., Wang, W., Feng, Y., 2022. Politicization of the hydropower dams in the Lancang-Mekong Basin: a review of contemporary environmental challenges. Energies 15, 1682. https://doi.org/10.3390/en15051682.

Hecht, J.S., Lacombe, G., Arias, M.E., Dang, T.D., Piman, T., 2019. Hydropower dams of the Mekong River basin: a review of their hydrological impacts. J. Hydrol. 568, 285–300. https://doi.org/10.1016/j.jhydrol.2018.10.045.

Hoang, L.P., van Vliet, M.T.H., Kummu, M., Lauri, H., Koponen, J., Supit, I., Leemans, R., Kabat, P., Ludwig, F., 2019. The Mekong's future flows under multiple drivers: how climate change, hydropower developments and irrigation expansions drive hydrological changes. Sci. Total Environ. 649, 601–609. https://doi.org/10.1016/j.scitotenv.2018.08.160.

Hong, S.H., Wdowinski, S., 2011. Evaluation of the quad-polarimetric Radarsat-2 observations for the wetland InSAR application. Can. J. Remote. Sens. 37 (5), 484–492.

Huete, A.R., Liu, H.Q., Batchily, K., van Leeuwen, W., 1997. A comparison of vegetation indices over a global set of TM images for EOS-MODIS. Remote Sens. Environ. 59, 440–451.

Huffman, G.J., 2019. The transition in multi-satellite products from TRMM to GPM (TMPA to IMERG). Algoritm. Inf. Doc.

Johnston, R., Kummu, M., 2012. Water resource models in the Mekong Basin: a review. Water Resour. Manag. 26, 429–455. https://doi.org/10.1007/s11269-011-9925-8.

Jolliffe, I.T., Cadima, J., 2016. Principal component analysis: a review and recent developments. Philos. Trans. R. Soc. A Math. Phys. Eng. Sci. 374, 20150202. https://doi.org/10.1098/rsta.2015.0202.

Kang, H., Sridhar, V., Ali, S.A., 2022. Climate change impacts on conventional and flash droughts in the Mekong River basin. Sci. Total Environ. 838, 155845.

Kim, J.-W., Yeh, S.-W., Chang, E.-C., 2014. Combined effect of El Niño-southern oscillation and Pacific decadal oscillation on the east Asian winter monsoon. Clim. Dyn. 42, 957–971. https://doi.org/10.1007/s00382-013-1730-z.

Kondolf, G.M., Rubin, Z.K., Minear, J.T., 2014. Dams on the Mekong: cumulative sediment starvation. Water Resour. Res. 50, 5158–5169. https://doi.org/10.1002/2013WR014651.

Kreibich, H., Van Loon, A.F., Schröter, K., Ward, P.J., Mazzoleni, M., Sairam, N., Abeshu, G.W., Agafonova, S., AghaKouchak, A., Aksoy, H., Alvarez-Garreton, C., Aznar, B., Balkhi, L., Barendrecht, M.H., Biancamaria, S., Bos-Burgering, L., Bradley, C., Budiyono, Y., Buytaert, W., Capewell, L., Carlson, H., Cavus, Y., Couasnon, A., Coxon, G., Daliakopoulos, I., de Ruiter, M.C., Delus, C., Erfurt, M., Esposito, G., François, D., Frappart, F., Freer, J., Frolova, N., Gain, A.K., Grillakis, M., Grima, J.O., Guzmán, D.A., Huning, L.S., Ionita, M., Kharlamov, M., Khoi, D.N., Kieboom, N., Kireeva, M., Koutroulis, A., Lavado-Casimiro, W., Li, H.-Y., Lasat, M.C., Macdonald, D., Mård, J., Mathew-Richards, H., McKenzie, A., Mejia, A., Mendiondo, E.M., Mens, M., Mobini, S., Mohor, G.S., Nagavciuc, V., Ngo-Duc, T., Thao Nguyen Huynh, T., Nhi, P.T.T., Petrucci, O., Nguyen, H.Q., Quintana-Seguí, P., Razavi, S., Ridolfi, E., Riegel, J., Sadik, M.S., Savelli, E., Sazonov, A., Sharma, S., Sörensen, J., Arguello Souza, F.A., Stahl, K., Steinhausen, M., Stoelzle, M., Szalińska, W., Tang, Q., Tian, F., Tokarczyk, T., Tovar, C., Tran, T.V.T., Van Huijgevoort, M.H.J., van Vliet, M.T.H., Vorogushyn, S., Wagener, T., Wang, Y., Wendt, D.E., Wickham, E., Yang, L., Zambrano-Bigiarini, M., Blöschl, G., Di Baldassarre, G., 2022. The challenge of unprecedented floods and droughts in risk management. Nature 608, 80–86. https://doi.org/10.1038/s41586-022-04917-5.

Kreibich, H., Schröter, K., Di Baldassarre, G., Van Loon, A., Mazzoleni, M., Abeshu, G.W., Ward, P.J., 2023. Panta Rhei benchmark dataset: socio-hydrological data of paired events of floods and droughts. Earth System Science Data Discussions 2023, 1–27.
Kuenzer, C., Guo, H., Huth, J., Leinenkugel, P., Li, X., Dech, S., 2013. Flood mapping and flood dynamics of the Mekong Delta: ENVISAT-ASAR-WSM based time series analyses. Remote Sens. 5 (2), 687–715.
Kummu, M., Sarkkula, J., 2008. Impact of the Mekong River Flow Alteration on the Tonle Sap Flood Pulse. ambi 37, 185–192. https://doi.org/10.1579/0044-7447(2008)37[185:IOTMRF]2.0.CO;2.
Kummu, M., Varis, O., 2007. Sediment-related impacts due to upstream reservoir trapping, the lower Mekong River. Geomorphology 85, 275–293. https://doi.org/10.1016/j.geomorph.2006.03.024.
Lauri, H., de Moel, H., Ward, P.J., Räsänen, T.A., Keskinen, M., Kummu, M., 2012. Future changes in Mekong River hydrology: impact of climate change and reservoir operation on discharge. Hydrol. Earth Syst. Sci. 16, 4603–4619. https://doi.org/10.5194/hess-16-4603-2012.
Lever, J., Krzywinski, M., Altman, N., 2017. Principal component analysis. Nat. Methods 14, 641–642. https://doi.org/10.1038/nmeth.4346.
Li, X., Liu, J.P., Saito, Y., Nguyen, V.L., 2017. Recent evolution of the Mekong Delta and the impacts of dams. Earth Sci. Rev. 175, 1–17. https://doi.org/10.1016/j.earscirev.2017.10.008.
Li, Y., Lu, H., Yang, K., Wang, W., Tang, Q., Khem, S., Huang, Y., 2021. Meteorological and hydrological droughts in Mekong River basin and surrounding areas under climate change. J. Hydrol. Region. Stud. 36, 100873.
Lu, X.X., Chua, S.D.X., 2021. River discharge and water level changes in the Mekong River: droughts in an era of Mega-Dams. Hydrol. Process. 35 https://doi.org/10.1002/hyp.14265.
Lu, L., Fan, H., Liu, J., Liu, J., Yin, J., 2019. Time series mining subsidence monitoring with temporarily coherent points interferometry synthetic aperture radar: a case study in Peixian, China. Environ. Earth Sci. 78, 1–17.
Mantua, N.J., Hare, S.R., Zhang, Y., Wallace, J.M., Francis, R.C., 1997. A Pacific Interdecadal climate oscillation with impacts on Salmon production. Bull. Amer. Meteor. Soc. 78, 1069–1079. https://doi.org/10.1175/1520-0477(1997)078<1069:APICOW>2.0.CO;2.
Martens, B., Miralles, D.G., Lievens, H., van der Schalie, R., de Jeu, R.A.M., Férnandez-Prieto, D., Beck, H.E., Dorigo, W.A., Verhoest, N.E.C., 2016. GLEAM v3: satellite-based land evaporation and root-zone soil moisture (preprint). Hydrology. https://doi.org/10.5194/gmd-2016-162.
Miralles, D.G., Holmes, T.R.H., De Jeu, R.A.M., Gash, J.H., Meesters, A.G.C.A., Dolman, A.J., 2011. Global land-surface evaporation estimated from satellite-based observations. Hydrol. Earth Syst. Sci. 15, 453–469. https://doi.org/10.5194/hess-15-453-2011.
Nguyen, T.-T.-H., Li, M.-H., Vu, T.M., Chen, P.-Y., 2023. Multiple drought indices and their teleconnections with ENSO in various spatiotemporal scales over the Mekong River basin. Sci. Total Environ. 854, 158589 https://doi.org/10.1016/j.scitotenv.2022.158589.
Nilsson, C., Reidy, C.A., Dynesius, M., Revenga, C., 2005. Fragmentation and flow regulation of the World's large river systems. Science 308, 405–408. https://doi.org/10.1126/science.1107887.
Normandin, C., Frappart, F., Diepkilé, A.T., Marieu, V., Mougin, E., Blarel, F., Lubac, B., Braquet, N., Ba, A., 2018a. Evolution of the performances of radar altimetry Missions from ERS-2 to sentinel-3A over the inner Niger Delta. Remote Sens. 10, 833. https://doi.org/10.3390/rs10060833.
Normandin, C., Frappart, F., Lubac, B., Bélanger, S., Marieu, V., Blarel, F., Robinet, A., Guiastrennec-Faugas, L., 2018b. Quantification of surface water volume changes in the Mackenzie Delta using satellite multi-mission data. Hydrol. Earth Syst. Sci. 22, 1543–1561. https://doi.org/10.5194/hess-22-1543-2018.
Normandin, C., Frappart, F., Bourrel, L., Diepkilé, A.T., Mougin, E., Zwarts, L., Wigneron, J.P., 2024. Quantification of surface water extent and volume in the inner Niger Delta (IND) over 2000–2022 using multispectral imagery and radar altimetry. Geocarto Int. 39 (1), 2311203.
Papa, F., Frappart, F., 2021. Surface water storage in rivers and wetlands derived from satellite observations: a review of current advances and future opportunities for hydrological sciences. Remote Sens. 13 (20), 4162.
Papa, F., Frappart, F., Malbeteau, Y., Shamsudduha, M., Vuruputur, V., Sekhar, M., Calmant, S., 2015. Satellite-derived surface and sub-surface water storage in the Ganges Brahmaputra River basin. J. Hydrol. Region. Stud. 4, 15–35.
Peñas, F.J., Barquín, J., 2019. Assessment of large-scale patterns of hydrological alteration caused by dams. J. Hydrol. 572, 706–718. https://doi.org/10.1016/j.jhydrol.2019.03.056.
Pezzulli, S., Stephenson, D.B., Hannachi, A., 2005. The variability of seasonality. J. Clim. 18, 71–88.
Pham-Duc, B., 2018. *Satellite remote sensing of the variability of the continental hydrology cycle in the lower Mekong basin over the last two decades* (Doctoral dissertation, Sorbonne université).
Pham-Duc, B., Prigent, C., Aires, F., 2017. Surface water monitoring within Cambodia and the Vietnamese Mekong Delta over a year, with Sentinel-1 SAR observations. Water *9* (6), 366.
Pham-Duc, B., Papa, F., Prigent, C., Aires, F., Biancamaria, S., Frappart, F., 2019. Variations of surface and subsurface water storage in the lower Mekong Basin (Vietnam and Cambodia) from multisatellite observations. Water 11, 75. https://doi.org/10.3390/w11010075.
Piman, T., Lennaerts, T., Southalack, P., 2013. Assessment of hydrological changes in the lower Mekong Basin from basin-wide development scenarios: ASSESSMENT OF HYDROLOGICAL CHANGES IN THE LOWER MEKONG BASIN. Hydrol. Process. 27, 2115–2125. https://doi.org/10.1002/hyp.9764.
Poff, N.L., Schmidt, J.C., 2016. How dams can go with the flow. Science 353, 1099–1100. https://doi.org/10.1126/science.aah4926.
Pokhrel, Y., Burbano, M., Roush, J., Kang, H., Sridhar, V., Hyndman, D., 2018. A review of the integrated effects of changing climate, land use, and dams on Mekong River hydrology. Water 10, 266. https://doi.org/10.3390/w10030266.
Poortinga, A., Aekakkararungroj, A., Kityuttachai, K., Nguyen, Q., Bhandari, B., Soe Thwal, N., Priestley, H., Kim, J., Tenneson, K., Chishtie, F., Towashiraporn, P., Saah, D., 2020. Predictive analytics for identifying land cover change hotspots in the Mekong region. Remote Sens. 12, 1472. https://doi.org/10.3390/rs12091472.
Prakongsri, P., Santiboon, T., 2020. Effective water resources Management for Communities in the Chi River basin in Thailand. Environ. Claims J. 32, 323–348. https://doi.org/10.1080/10406026.2020.1765529.
Prigent, C., Jimenez, C., Bousquet, P., 2020. Satellite-derived global surface water extent and dynamics over the last 25 years (GIEMS-2). J. Geophys. Res. Atmos. 125 (3), e2019JD030711.
R, P., 1988. Principal component analysis in meteorology and oceanography. Elsevier Sci. Publ. 17, 425.
Räsänen, T.A., Someth, P., Lauri, H., Koponen, J., Sarkkula, J., Kummu, M., 2017. Observed river discharge changes due to hydropower operations in the upper Mekong Basin. J. Hydrol. 545, 28–41. https://doi.org/10.1016/j.jhydrol.2016.12.023.
Rayner, N.A., 2003. Global analyses of sea surface temperature, sea ice, and night marine air temperature since the late nineteenth century. J. Geophys. Res. 108, 4407. https://doi.org/10.1029/2002JD002670.
Saah, D., Tenneson, K., Poortinga, A., Nguyen, Q., Chishtie, F., Aung, K.S., Markert, K.N., Clinton, N., Anderson, E.R., Cutter, P., Goldstein, J., Housman, I.W., Bhandari, B., Potapov, P.V., Matin, M., Uddin, K., Pham, H.N., Khanal, N., Maharjan, S., Ellenberg, W.L., Bajracharya, B., Bhargava, R., Maus, P., Patterson, M., Flores-Anderson, A.I., Silverman, J., Sovann, C., Do, P.M., Nguyen, G.V., Bounthabandit, S., Aryal, R.R., Myat, S.M., Sato, K., Lindquist, E., Kono, M., Broadhead, J., Towashiraporn, P., Ganz, D., 2020. Primitives as building blocks for constructing land cover maps. Int. J. Appl. Earth Obs. Geoinf. 85, 101979 https://doi.org/10.1016/j.jag.2019.101979.
Sakamoto, T., Van Nguyen, N., Kotera, A., Ohno, H., Ishitsuka, N., Yokozawa, M., 2007. Detecting temporal changes in the extent of annual flooding within the Cambodia and the Vietnamese Mekong Delta from MODIS time-series imagery. Remote Sens. Environ. 109, 295–313. https://doi.org/10.1016/j.rse.2007.01.011.
Schwatke, C., Halicki, M., Scherer, D., 2024. Generation of high-resolution water surface slopes from multi-mission satellite altimetry. Water Resour. Res. 60 (5), e2023WR034907.
Shiklomanov, I.A., Rodda, J.C., 2003. World Water Resources at the Beginning of the Twenty-First Century. Cambridge University Press.
Shu, S., Liu, H., Beck, R.A., Frappart, F., Korhonen, J., Lan, M., Huang, Y., 2021. Evaluation of historic and operational satellite radar altimetry missions for constructing consistent long- term lake water level records. Hydrol. Earth Syst. Sci. 25 (3), 1643–1670.
Stone, R., 2016. Dam-building threatens Mekong fisheries. Science 354, 1084–1085. https://doi.org/10.1126/science.354.6316.1084.
Tang, Q., Yun, X., Wang, J., Deng, H., Liu, B., Tran, T.C., Gaffney, P.P., 2024. Water hazards: Drought and flood. In: Water Resources in the Lancang-Mekong River Basin: Impact of Climate Change and Human Interventions. Singapore, Springer Nature Singapore, pp. 255–281.
Thilakarathne, M., Sridhar, V., 2017. Characterization of future drought conditions in the lower Mekong River basin. Weather and Climate Extremes 17, 47–58.
Torrence, C., Compo, G.P., 1998. A practical guide to wavelet analysis. Bull. Am. Meteorol. Soc. 79, 61–78. https://doi.org/10.1175/1520-0477(1998)079<0061:APGTWA>2.0.CO;2.
Tourian, M.J., Tarpanelli, A., Elmi, O., Qin, T., Brocca, L., Moramarco, T., Sneeuw, N., 2016. Spatiotemporal densification of river water level time series by multimission satellite altimetry. Water Resour. Res. 52 (2), 1140–1159.
Tran, D.D., van Halsema, G., Hellegers, P.J., Ludwig, F., Wyatt, A., 2018. Questioning triple rice intensification on the Vietnamese mekong delta floodplains: an environmental and economic analysis of current land-use trends and alternatives. J. Environ. Manag. 217, 429–441.
Try, S., Tanaka, S., Tanaka, K., Sayama, T., Lee, G., Oeurng, C., 2020. Assessing the effects of climate change on flood inundation in the lower Mekong Basin using high-resolution AGCM outputs. Prog Earth Planet Sci 7, 1–16.
Van Kien, N., Hoang Han, N., Cramb, R., 2020. Trends in Rice-based farming Systems in the Mekong Delta. In: Cramb, R. (Ed.), White Gold: The Commercialisation of Rice Farming in the Lower Mekong Basin. Springer Nature Singapore, Singapore, pp. 347–373. https://doi.org/10.1007/978-981-15-0998-8_17.
Vantrepotte, V., Mélin, F., 2009. Temporal variability of 10-year global SeaWiFS time-series of phytoplankton chlorophyll a concentration. ICES J. Mar. Sci. 66, 1547–1556.
Vantrepotte, V., Loisel, H., Mélin, F., Desailly, D., Duforêt-Gaurier, L., 2011. Global particulate matter pool temporal variability over the SeaWiFS period (1997-2007): GLOBAL PARTICULATE MATTER VARIABILITY. Geophys. Res. Lett. 38, n/a–n/a. https://doi.org/10.1029/2010GL046167.
Västilä, K., Kummu, M., Sangmanee, C., Chinvanno, S., 2010. Modelling climate change impacts on the flood pulse in the lower Mekong floodplains. J. Water Clim. Change 1, 67–86. https://doi.org/10.2166/wcc.2010.008.
Vu, H.T.D., Tran, D.D., Schenk, A., Nguyen, C.P., Vu, H.L., Oberle, P., Trinh, V.C., Nestmann, F., 2022a. Land use change in the Vietnamese Mekong Delta: new evidence from remote sensing. Sci. Total Environ. 813, 151918 https://doi.org/10.1016/j.scitotenv.2021.151918.

Vu, H.T.D., Vu, H.L., Oberle, P., Andreas, S., Nguyen, P.C., Tran, D.D., 2022b. Datasets of land use change and flood dynamics in the vietnamese mekong delta. Data Brief 42, 108268. https://doi.org/10.1016/j.dib.2022.108268.

Wdowinski, S., Amelung, F., Kim, S.W., Dixon, T., 2015. Wetland InSAR. In: Remote Sensing of Wetlands: Applications and Advances. CRC Press, Boca Raton, FL, USA, p. 137.

Wei, Y., Wei, J., Li, G., Wu, S., Yu, D., Ghoreishi, M., Lu, Y., Souza, F.A.A., Sivapalan, M., Tian, F., 2022. A socio-hydrological framework for understanding conflict and cooperation with respect to transboundary rivers. Hydrol. Earth Syst. Sci. 26, 2131–2146. https://doi.org/10.5194/hess-26-2131-2022.

Winemiller, K.O., McIntyre, P.B., Castello, L., Fluet-Chouinard, E., Giarrizzo, T., Nam, S., Baird, I.G., Darwall, W., Lujan, N.K., Harrison, I., Stiassny, M.L.J., Silvano, R.A.M., Fitzgerald, D.B., Pelicice, F.M., Agostinho, A.A., Gomes, L.C., Albert, J.S., Baran, E., Petrere, M., Zarfl, C., Mulligan, M., Sullivan, J.P., Arantes, C.C., Sousa, L.M., Koning, A.A., Hoeinghaus, D.J., Sabaj, M., Lundberg, J.G., Armbruster, J., Thieme, M.L., Petry, P., Zuanon, J., Vilara, G.T., Snoeks, J., Ou, C., Rainboth, W., Pavanelli, C.S., Akama, A., Soesbergen, A. van, Sáenz, L., 2016. Balancing hydropower and biodiversity in the Amazon, Congo, and Mekong. Science 351, 128–129. doi: https://doi.org/10.1126/science.aac7082.

Xiao, X., Boles, S., Liu, J., Zhuang, D., Frolking, S., Li, C., Salas, W., Moore, B., 2005. Mapping paddy rice agriculture in southern China using multi-temporal MODIS images. Remote Sens. Environ. 95, 480–492. https://doi.org/10.1016/j.rse.2004.12.009.

Yoshida, Y., Lee, H.S., Trung, B.H., Tran, H.-D., Lall, M.K., Kakar, K., Xuan, T.D., 2020. Impacts of mainstream hydropower dams on fisheries and agriculture in lower Mekong Basin. Sustainability 12, 2408. https://doi.org/10.3390/su12062408.

Zarfl, C., Lumsdon, A.E., Berlekamp, J., Tydecks, L., Tockner, K., 2015. A global boom in hydropower dam construction. Aquat. Sci. 77, 161–170. https://doi.org/10.1007/s00027-014-0377-0.

Ziv, G., Baran, E., Nam, S., Rodríguez-Iturbe, I., Levin, S.A., 2012. Trading-off fish biodiversity, food security, and hydropower in the Mekong River basin. Proc. Natl. Acad. Sci. USA 109, 5609–5614. https://doi.org/10.1073/pnas.1201423109.